https://doi.org/10.1093/plcell/koad141 THE PLANT CELL 2023: 35: 3504–3521

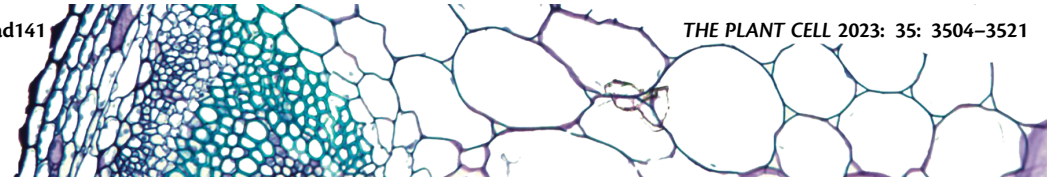

Research Article

Phosphorylation of ADAPTOR PROTEIN-2 μ-adaptin by ADAPTOR-ASSOCIATED KINASE1 regulates the tropic growth of Arabidopsis roots

Wei Siao [1,2] Peng Wang [1,2] Xiuyang Zhao [1,2] Lam Dai Vu [1,2] Ive De Smet [1,2] and Eugenia Russinova [1,2,*,†]

1 Department of Plant Biotechnology and Bioinformatics, Ghent University, 9052 Ghent, Belgium
2 Center for Plant Systems Biology, VIB, 9052 Ghent, Belgium

*Author for correspondence: eurus@psb.ugent.be
†Senior author
The author responsible for distribution of materials integral to the findings presented in this article in accordance with the policy described in the instructions for Authors (https://academic.oup.com/plcell/pages/General-Instructions) is: Eugenia Russinova (eurus@psb.vib-ugent.be).

Abstract

ADAPTOR-ASSOCIATED PROTEIN KINASE1 (AAK1) is a known regulator of clathrin-mediated endocytosis in mammals. Human AAK1 phosphorylates the μ2 subunit of the ADAPTOR PROTEIN-2 (AP-2) complex (AP2M) and plays important roles in cell differentiation and development. Previous interactome studies discovered the association of AAK1 with AP-2 in Arabidopsis (*Arabidopsis thaliana*), but its function was unclear. Here, genetic analysis revealed that the Arabidopsis *aak1* and *ap2m* mutants both displayed altered root tropic growth, including impaired touch- and gravity-sensing responses. In Arabidopsis, AAK1-phosphorylated AP2M on Thr-163, and expression of the phospho-null version of AP2M in the *ap2m* mutant led to an *aak1*-like phenotype, whereas the phospho-mimic forms of AP2M rescued the *aak1* mutant. In addition, we found that the AAK1-dependent phosphorylation state of AP2M modulates the frequency distribution of endocytosis. Our data indicate that the phosphorylation of AP2M on Thr-163 by AAK1 fine-tunes endocytosis in the Arabidopsis root to control its tropic growth.

Introduction

The dynamic turnover of plasma membrane (PM) proteins is tightly regulated by the rates of endocytosis, degradation, and protein delivery to the PM via secretion or recycling. The best-characterized route for PM protein internalization is clathrin-mediated endocytosis (CME) through clathrin-coated vesicles (CCVs) (Traub 2009; McMahon and Boucrot 2011). In mammalian cells, CCVs develop from clathrin-coated pits that are formed by the assembly of the major coat proteins clathrin and ADAPTOR PROTEIN-2 (AP-2) (Roth and Porter 1964; Kirchhausen et al. 2014). Low amounts of other clathrin adaptors and CME accessory proteins are also found in CCVs that function as scaffolds, cargo recruiters, membrane curvature generators, and CME regulators (Borner et al. 2012; Mettlen et al. 2018).

The mammalian heterotetrameric AP-2 complex consists of two large subunits (α2 and β2), one medium subunit (μ2), and one small subunit (σ2). By binding to phosphatidylinositol 4,5-bisphosphate (PIP2), the inactive, closed form of cytosolic AP-2 is initially recruited to the PM, where AP-2 is conformationally changed to an active, open form that is favored by phosphorylation on Thr-156 in the μ2 subunit (Collins et al. 2002; Höning et al. 2005). Previous data suggest that phosphorylation of the human μ2 enhances binding to phospholipids and cargoes (Ricotta et al. 2002; Höning et al. 2005) and that mutation in the phosphorylation site inhibits transferrin uptake (Olusanya et al. 2001). However, later studies have shown that, although μ2 Thr-156 phosphorylation stabilizes the open form of AP-2, unphosphorylated AP-2 can readily bind to cargo-containing membranes, and its cargo affinity is not enhanced by the Thr-156

Received November 16, 2022. Accepted April 21, 2023. Advance access publication July 13, 2023

IN A NUTSHELL

Background: Plant roots react to their environment by using hormone signaling pathways, which enable their cells to respond to external cues such as gravity and soil properties. Endocytosis is a cellular process in which membrane proteins or other external substances are internalized, and it can affect hormone signaling and cell communication. Therefore, changes in endocytosis can impact how a plant root responds to external stimuli. Understanding the role of endocytosis in plant root behavior can be useful in developing effective strategies to improve plant root growth and enhance nutrient-seeking behavior in the soil.

Questions: Is there a mechanism that can regulate components of the endocytic machinery? Can phosphorylation, a post-translational modification, be involved in this process?

Findings: ADAPTOR-ASSOCIATED PROTEIN KINASE1 (AAK1) phosphorylates the medium subunit of the adaptor protein-2 complex (AP2M), on a single amino acid residue. Mutations in the *AAK1* gene or prevention of AP2M phosphorylation in Arabidopsis alter the root gravitropism and touch responses to hard surfaces. Introducing a phosphomimic form of AP2M into an *aak1* mutant restored the altered root behavior to the wild-type level. Our findings show that a single phosphorylation event on AP2M by AAK1 can modify root behavior while maintaining normal plant growth and development.

Next steps: Scientists are working to decode the complex behavior of roots to enhance their ability to adapt to different and changing soil environments. Future studies will investigate how endocytosis coordinates different signaling pathways involved in various root tropisms, as well as identify new regulators of endocytosis that can affect root behavior.

phosphorylation of μ2 (Jackson et al. 2010; Kelly et al. 2014; Kadlecova et al. 2016; Wrobel et al. 2019).

The NUMB-ASSOCIATED KINASE (NAK) family member ADAPTOR-ASSOCIATED KINASE1 (AAK1) phosphorylated μ2 in vitro and copurified with AP-2 in CCVs in human cells (Conner and Schmid 2002; Ricotta et al. 2002; Borner et al. 2012; Sorrell et al. 2016). However, gene silencing of *AAK1* did not alter the AP-2 phosphorylation status in cells, and AAK1-phosphorylated Thr-156 in μ2 negatively regulated the AP2-dependent endocytosis of transferrin (Conner and Schmid 2002, 2003; Henderson and Conner 2007; Partlow et al. 2019). Through control of CME, the human AAK1 negatively regulates the β-catenin-dependent Wnt signaling pathway that regulates key cellular functions including proliferation, differentiation, migration, genetic stability, apoptosis, and stem cell renewal (Agajanian et al. 2019) and positively regulates the Notch signaling pathway that is important for cell-cell communication (Gupta-Rossi et al. 2011), both pathways involving cell-surface receptors activated by specific ligands. Silencing of *AAK1* also interfered with some AP2-independent events, such as accumulation of transferrin receptors in perinuclear endosomes, vesicular stomatitis virus entry, and the low-density lipoprotein (LDL) uptake (Pelkmans et al. 2005; Henderson and Conner 2007). Hence, human AAK1 plays multiple roles in different pathways.

Recently, a crystal structure study identified an open and active conformation of AP-2, designated open+, of which the "bowl" (α trunk, β2 trunk, μ2 N-terminus, and σ2) superimposed well with that of the open form (Wrobel et al. 2019). The main difference between the open and open+ conformers is the different orientations of the μ2 C-terminus (Wrobel et al. 2019). In the current mammalian model, unphosphorylated AP-2 is already in equilibrium between the open and open+ forms on the PM, with the open+ form only compatible with the Thr-156 phosphorylation in μ2 (Kelly et al. 2014; Wrobel et al. 2019). Therefore, the Thr-156 phosphorylation in μ2 affects clathrin-coated pit maturation and the CME rate because of the stabilizing ability of the open+ cargo-binding conformation of AP-2, but does not alter the efficiency of cargo sequestration (Wrobel et al. 2019).

In Arabidopsis (*Arabidopsis thaliana*), AP-2, which consists of two large subunits (AP2A and AP2B), one medium subunit (AP2M) and one small subunit (AP2S), also facilitates CME of various PM proteins (Di Rubbo et al. 2013; Kim et al. 2013; Yoshinari et al. 2019; Liu et al. 2020). In contrast to the embryo lethal phenotype of a single *ap2* subunit knockout mutant in mouse (*Mus musculus*) (Mitsunari et al. 2005), Arabidopsis mutants in single subunits of AP-2 display relatively mild growth phenotypes, such as slender rosette leaves, short petioles, defects in staminal filament and pollen tube elongation, and reduced fertility (Di Rubbo et al. 2013; Fan et al. 2013; Kim et al. 2013; Yamaoka et al. 2013). A recent interactome study identified AAK1 as a binding partner of AP-2 in Arabidopsis (Wang et al. 2023), but the function of AAK1 as well as the phospho-regulation of AP2M, remain unclear.

Here, we show that Arabidopsis AAK1 is an active serine/threonine kinase that can phosphorylate AP2M on Thr-163 in vitro. The knockout of *AAK1* altered the tropic growth of roots due to decreased waving, reduced gravitropic bending, and enhanced obstacle avoidance, whereas the knockout of *AP2M* resulted in aberrant root behavior, namely,

increased waving, skewing, agravitropism, and root curling when impenetrable surfaces were encountered. By means of genetic studies, we reveal that the phosphorylation of AP2M on Thr-163 *in planta* determines root behavior. We also demonstrate that AAK1 maintains the balance of endocytosis in root cells and fine-tunes AP2M function via phosphorylation.

Results

Arabidopsis AAK1 is an active kinase that phosphorylates AP2M on Thr-163 in vitro

Previously, in an interactome study, we identified a protein kinase superfamily protein (AT2G32850) that copurified specifically with AP-2 and was orthologous to the mammalian AAK1 (Wang et al. 2023). Phylogenetic analysis across eukaryotic species indicated that contrary to the mammalian *AAK1* gene, which belongs to the highly diverse NAK family (Sorrell et al. 2016) and *AAK1* genes in other plant species such as maize (*Zea mays*) and rice (*Oryza sativa*), which are present in duplicate copies, Arabidopsis *AAK1* is a single-copy gene (Supplemental Fig. S1A). Similar to human AAK1 (Conner and Schmid 2002), Arabidopsis AAK1 contains an N-terminal kinase domain and two adaptin-binding motifs (WXXFXD and WXXF) in its C-terminus (Fig. 1A), but the QP-rich middle domain is replaced by a coiled-coil domain (Fig. 1A; Supplemental Fig. S1B). The kinase domain of Arabidopsis AAK1 is 43% identical and 62% similar to that of human AAK1, and the catalytic sites are well conserved (Supplemental Fig. S1C). The protein domain structure and the association with AP-2 (Wang et al. 2023) suggest that Arabidopsis AAK1 might also function as an AP-2 kinase.

To test whether Arabidopsis AAK1 is an active kinase, we generated maltose-binding protein (MBP)-tagged recombinant proteins of wild-type AAK1 (MBP-AAK1) and two putative AAK1 kinase-dead versions (MBP-AAK1^{K57A} and MBP-AAK1^{D157A}) by mutating the conserved residues within the kinase domain (Conner and Schmid 2003) (Fig. 1A; Supplemental Fig. S1C). An in vitro kinase assay revealed that wild-type AAK1 exhibited autophosphorylation activity, whereas the two kinase-dead versions of AAK1 did not (Fig. 1B), implying that AAK1 is an active kinase.

Human AAK1 phosphorylates the μ2 subunit of AP-2 at a single Thr-156 residue (Ricotta et al. 2002) that is conserved with Thr-163 in Arabidopsis AP2M (Fig. 1C). Searches in the Plant PTM Viewer (https://www.psb.ugent.be/webtools/ptm-viewer) (Vu et al. 2016; Willems et al. 2019) and PhosPhAt (https://phosphat.uni-hohenheim.de/db.html) (Zulawski et al. 2013) databases indicated the occurrence of three phosphorylated residues of AP2M *in planta* (Thr-163, Thr-159, and Ser-144) (Mergner et al. 2020) (Supplemental Fig. S2A). To determine whether Arabidopsis AAK1 can phosphorylate AP2M, we carried out an in vitro kinase assay with bacterially produced glutathione S-transferase (GST)-tagged AP2M and MBP-tagged AAK1 but did not detect phosphorylation on GST-AP2M (Supplemental Fig. S2B), probably because the recombinant AP2M protein either did not fold properly or the phosphorylation residue was inaccessible to AAK1.

Using a short synthetic peptide fused with a GST tag containing Thr-159 and Thr-163 residues (GST-AP2M-T163), we tested whether AAK1 phosphorylates the Thr-163 residue in AP2M. The in vitro kinase assay demonstrated that the short peptide was phosphorylated, whereas the GST fusion protein bearing a mutated peptide in which only the Thr-163 had been substituted with alanine (GST-AP2M-T163A) was not (Fig. 1D). However, phosphorylation on Thr-163 in the GST-AP2M-T163 peptide was not identified by mass spectrometry (MS) (Supplemental Data Set 1), likely due to technical limitations. Altogether, our data demonstrate that AAK1 phosphorylates AP2M on Thr-163 but not Thr-159 in vitro.

AAK1 regulates root waving and gravitropism in Arabidopsis

We next assessed the function of AAK1 in Arabidopsis. Analysis of transgenic Arabidopsis plants harboring the *pAAK1:nlsGFP* reporter revealed that *AAK1* is ubiquitously expressed in roots (Supplemental Fig. S3, A to C). Subsequently, we identified one T-DNA insertion mutant of *AAK1* (SALK_001684) (Fig. 2A) and generated transgenic plants overproducing the kinase by transforming wild-type Arabidopsis with *AAK1* genomic DNA driven by the cauliflower mosaic virus *(CaMV) 35S* promoter. Immunoblot analysis with a specific α-AAK1 antibody revealed that the SALK_001684 allele (hereafter designated *aak1-1*) was a knockout mutant and that the overexpression (OE) line (hereafter designated AAK1OE) accumulated more AAK1 protein than the wild-type accession, Columbia-0 (Col-0) (Fig. 2B). Neither the *aak1-1* mutant nor AAK1OE plants displayed any obvious growth defects throughout the vegetative and reproductive stages (Supplemental Fig. S4, A and B). Interestingly, 5-day-old *aak1-1* and AAK1OE seedlings had fewer and more wavy primary roots than the wild-type, respectively, whereas the primary root length of the two genotypes was similar to that of the wild-type (Fig. 2, C to E; Supplemental Data Set 2).

To confirm that the differences in root behavior resulted from AAK1 dysfunction, we deleted the *AAK1* gene by clustered regularly interspaced short palindromic repeats (CRISPR)/CRISPR-associated protein 9 (Cas9) technology from the 45th to 2359th bp (hereafter referred to as the *aak1-2* mutant; Fig. 2A). In addition to *aak1-2*, we also identified *aak1-3*, which had one nucleotide inserted 44 bp after the start codon, with a premature termination codon after the 29th amino acid as a consequence (Fig. 2A). No AAK1 protein was detected in *akk1-2* or *aak1-3* by immunoblotting with the α-AAK1 antibody (Fig. 2B), indicating that the two mutants were also knockout mutants. Like *aak1-1*, the primary roots of both 5-day-old *aak1-2* and *aak1-3* seedlings were less wavy than those of the wild-type (Fig. 2, C and E;

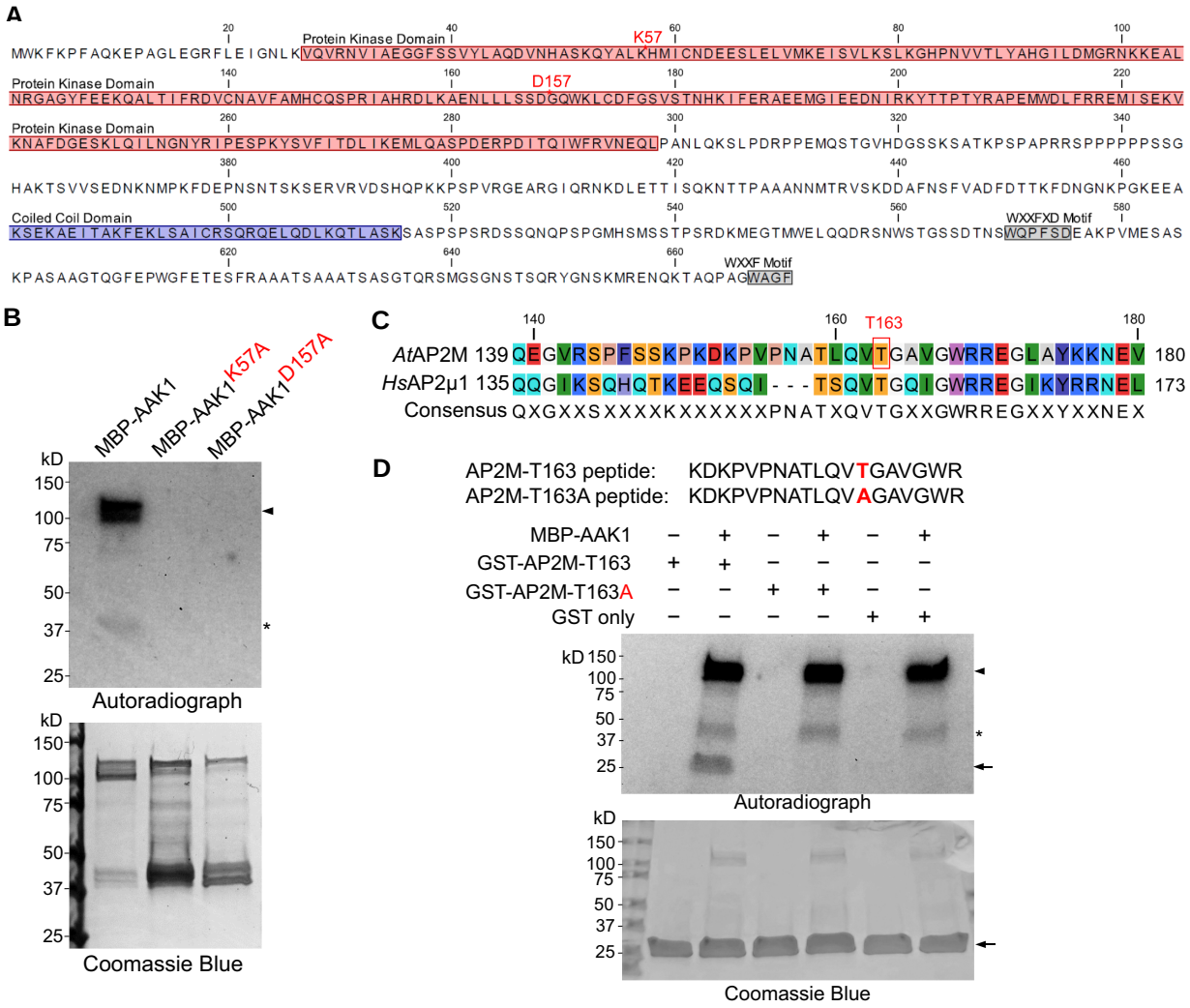

Figure 1. Arabidopsis AAK1 is an active kinase that phosphorylates AP2M on Thr-163 in vitro. **A)** Sequence and domain structures of Arabidopsis AAK1. The conserved lysine (K57) and aspartate (D157) that are important for nucleotide binding and catalysis are indicated. WXXFXD and WXXF are adaptin-binding motifs. **B)** In vitro kinase assay with isotope labeling. The MBP-AAK1 fusion protein can autophosphorylate in vitro when incubated with [^{32}P]-γ-ATP, whereas the kinase-dead versions of AAK1, MBP-AAK1^{K57A} and MBP- AAK1^{D157}, had no autophosphorylation activity. **C)** Amino acid alignment of Arabidopsis AP2M and human AP2µ1. The threonine (T) phosphorylation site at position 156 in human AP2µ1 is conserved in the Arabidopsis AP2M at position 163 (T163). **D)** In vitro kinase assay of the AP2M GST-tagged peptide containing Thr-163 (AP2M-T163) and the GST-tagged mutant peptide, in which the Thr-163 was substituted with alanine (AP2M-T163A). MBP-AAK1 was used as a kinase. The sequences of the short peptides (19 amino acids) are presented at the top. The GST protein was used as a negative control. Arrowheads and asterisks in **B** and **D)** indicate the autophosphorylation signal of MBP-AAK1 and nonspecific signals, respectively. Arrows in **D)** indicate the sizes of GST-AP2M-T163, GST-AP2M-T163A, and GST.

Supplemental Data Set 2), whereas the leaves and siliques developed normally (Supplemental Fig. S4, A and B). In addition to root waving, the early gravitropic responses were compromised in the *aak1* mutants (Fig. 2F; Supplemental Data Set 2; Supplemental Fig. S4C), thus hinting at impaired auxin transport. In agreement with this notion, the polarity of PIN2-green fluorescent protein (GFP) was moderately altered in the *aak1-1* root meristem (Supplemental Fig. S4, D and E; Supplemental Data Set 2).

To corroborate that the observed root phenotypes were caused by a mutation in the *AAK1* gene, we complemented the *aak1-1* mutant with a construct containing genomic *AAK1* DNA fused at the 3′ ends to the GFP gene under the control of the native *AAK1* promoter. Two independent homozygous transgenic lines, *pAAK1:AAK1-GFP/aak1-1* (lines #1 and #4) were characterized (Fig. 2B). Expression of AAK1-GFP in *aak1-1* restored the root waving and gravitropic bending back to those of the wild-type (Fig. 2, C to F; Supplemental Data Set 2), suggesting that the *pAAK1:AAK1-GFP* construct is functional.

Subsequently, we examined the subcellular localization of AAK1-GFP in *pAAK1:AAK1-GFP/aak1-1* line *#1* and

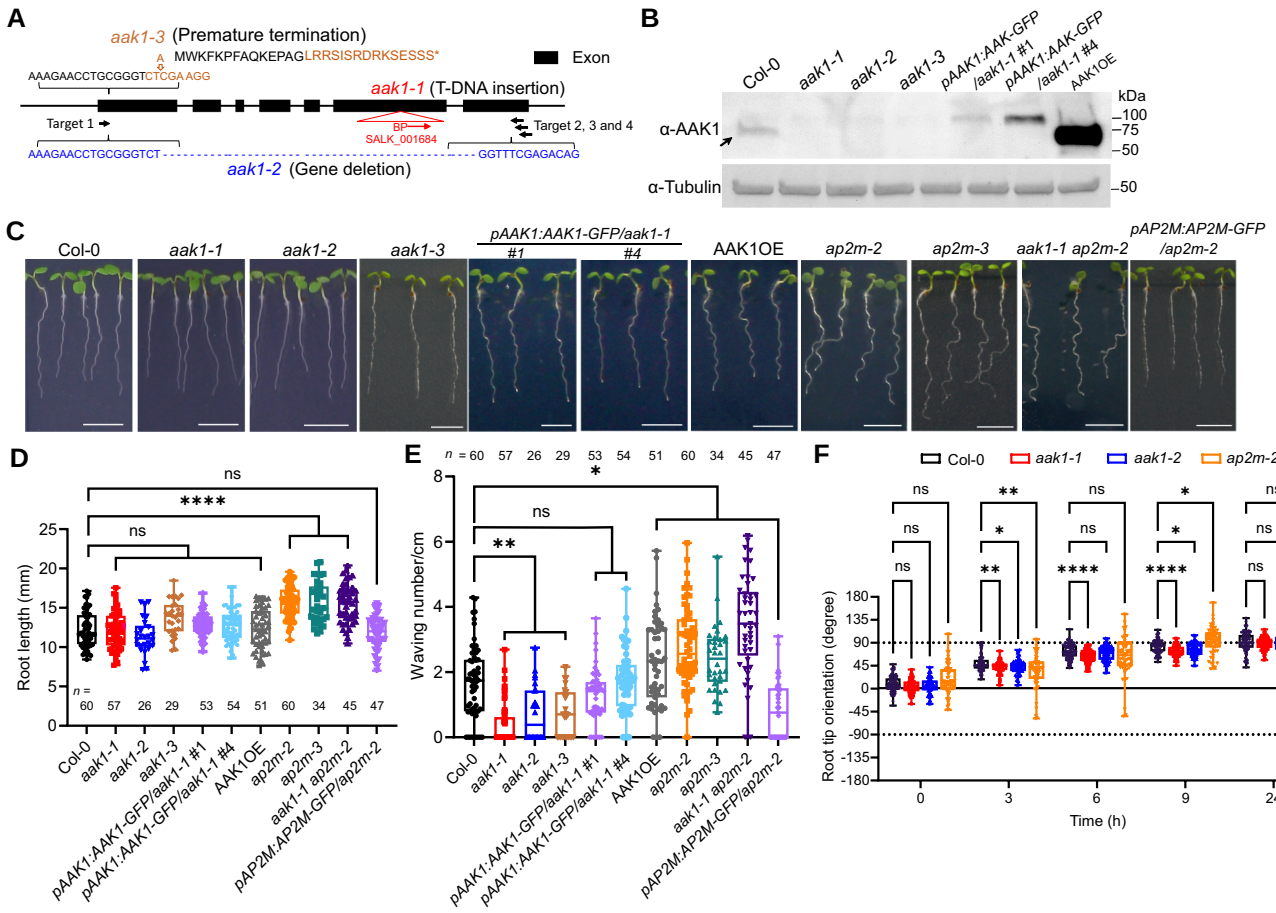

Figure 2. AAK1 and AP2M regulate root waving and gravitropism in Arabidopsis. **A)** Schematic representation of different *aak1* mutant alleles generated in this study. The locations of guide RNAs (gRNAs, black arrows) targeting the AAK1 locus are indicated. BP and Targets mark the T-DNA left border primer and the gDNA targeting sites, respectively. **B)** Immunoblot analysis of AAK1 protein levels in the wild-type (Col-0), *aak1-1*, *aak1-2*, *aak1-3* mutants, *pAAK1:AAP1-GFP/aak1-1* (lines #1 and #4), and the AAK1 overexpression line (*p35S:AAK1- GFP*/Col-0, AAK1OE) with the α-AAK1 antibody. Tubulin detected with α-tubulin antibody was used as a loading control. The arrow indicates endogenous AAK1. **C)** Root phenotypes of 5-day-old seedings of Col-0, *aak1-1*, *aak1-2*, *aak1-3* mutants, *pAAK1:AAP1-GFP/aak1-1* (lines #1 and #4), AAK1OE, and *ap2m-2* and *ap2m-3* mutants. Scale bar, 5 mm. **D)** Primary root length of each genotype as shown in **C)**. **E)** Root waving assay of each genotype as shown in **C)**. The root waviness was determined as the number of waves per root length. Three independent experiments were combined **D** and **E)**. **F)** Kinetics of the gravitropic bending of root tips of wild-type, *aak1-1*, *aak1-2*, and *ap2m-2* plotted against time after gravistimulation. Five-day-old seedlings grown vertically on the medium were gravistimulated by 90° rotation. Three independent experiments were combined, each with 20 to 30 roots per genotype in each experiment. The borders of boxes **D** to **F)** represent the 25th to 75th percentiles, the center horizontal line indicates the median, and the whiskers indicate the minimum and the maximum values. All individual values are plotted. *n*, number of roots **D** to **F)**. $^{*}P \leq 0.05$, $^{**}P \leq 0.01$, $^{****}P \leq 0.0001$ (one-way ANOVA in (**D** and **E)** and two-way ANOVA in (**F**)), ns, not significant.

determined that AAK1-GFP was mainly located in the cytoplasm. Although some punctate-like structures were observed (Supplemental Fig. S3, D to F), the structures are either transvacuolar strands or unevenly distributed in the cytoplasm (see Movie 1). To examine whether trace amounts of AAK1-GFP localized to the endosome, we stained the root cells with the dye FM4-64 (to monitor bulk endocytosis) while simultaneously treating them with the vesicle trafficking inhibitor brefeldin A (BFA). After 30 min of treatment, AAK1-GFP remained cytoplasmic without aggregation (Supplemental Fig. S3G), indicating that AAK1-GFP did not localize to the *trans*-Golgi network/early endosome. Time-lapse imaging of the PM (Supplemental Fig. S3H) revealed the lack of punctate signals, indicating that AAK1 functions in the cytoplasm. In summary, AAK1 is a ubiquitously expressed cytoplasmic kinase that controls primary root waving and gravity sensing during the seedling stage.

AP2M functions downstream of AAK1

Given that Arabidopsis AAK1 phosphorylated AP2M in vitro, we hypothesized that AAK1 regulates AP-2 function and, hence, that the root behavior of the *ap2m* mutant might also be affected. Although the *ap2m* mutant displayed a number of growth-related phenotypes (Kim et al. 2013; Yamaoka et al. 2013), no root phenotypes have been described. Interestingly, in contrast to the *aak1* mutants, the

primary root of the 5-day-old *ap2m-2* mutant exhibited enhanced waving and skewing and was longer than that of the wild-type (Fig. 2, C to E; Supplemental Data Set 2). To verify that these root phenotypes were due to the *AP2M* mutation, we generated an additional *ap2m* mutant by CRISPR/Cas9 technology. The resulting CRISPR/Cas9 mutant of *AP2M*, hereafter, designated *ap2m-3*, had a single nucleotide deleted 76 bp after the start codon, resulting in a premature stop codon after the 28th amino acid (Supplemental Fig. S4F). In addition to the previously reported growth phenotypes (Kim et al. 2013; Yamaoka et al. 2013), *ap2m-3* showed the same primary root phenotypes as *ap2m-2* (Fig. 2, C to E; Supplemental Data Set 2; Supplemental Fig. S4, A and B). The root gravitropic assay also revealed that the root bending angles of *ap2m-2* and *ap2m-3* deviated from the gravity vector (Fig. 2F; Supplemental Data Set 2; Supplemental Fig. S4C). Thus, AP2M regulates not only the growth and development of leaves and reproductive organs but also root behavior.

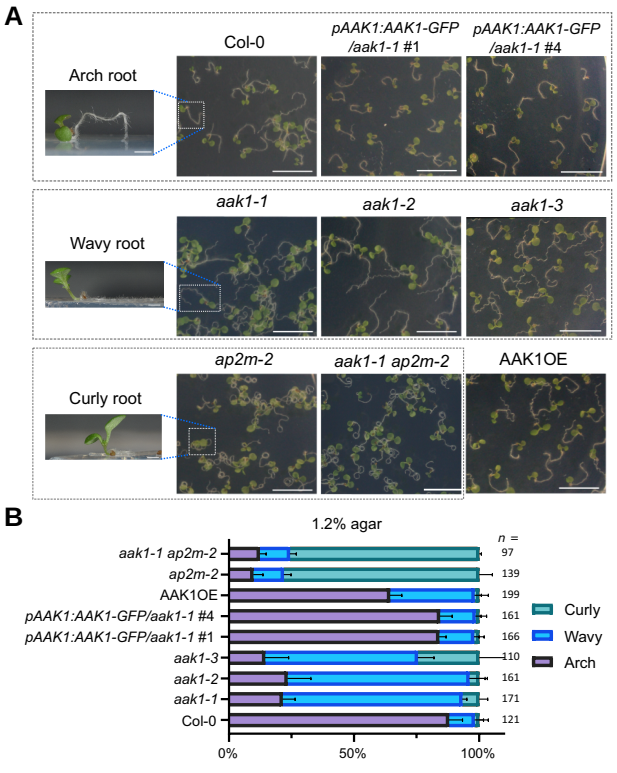

Figure 3. The primary roots of *aak1* and *ap2m* mutants exhibited distinct behaviors when grown on a surface of impenetrable agar. **A)** Representative images showing the root behavior (arch, wavy, and curly roots, as shown in the insets) of 7-day-old seedlings of wild-type (Col-0), *aak1- 1*, *aak1-2*, *aak1-3* mutants, *pAAK1:AAP1-GFP/aak1-1* (lines #1 and #4), the AAK1 overexpression line (*p35S:AAK1-GFP*/Col-0, AAK1OE), *ap2m-2* and *aak1-1 ap2m-2* mutants grown horizontally on 1.2% agar-containing medium. The genotypes with the same root behavior were grouped in dashed rectangles. Scale bars, 1 cm. **B)** Quantification of the root behavior of each genotype as in **A)**. Three independent experiments were combined. *n*, number of roots analyzed. Error bars represent the standard error (SE) of the three replicates.

As the root phenotypes pertaining to root waving differed in the *aak1* and *ap2m* mutants, we generated the *aak1-1 ap2m-2* double mutant and found that it exhibited root phenotypes similar to those of *ap2m-2*, including a longer primary root, an enhanced root waving and skewing behavior, disrupted root gravitropic bending, slender rosette leaves, shortened petioles, and reduced silique size (Fig. 2, C to E; Supplemental Data Set 2; Supplemental Fig. S4, A and B). Hence, *AP2M* is epistatic to *AAK1* and might be a downstream target. We also examined the root phenotype of the *pAP2M:AP2M-GFP/ap2m-2* complemented line, which rescued the leaf, flower, and silique phenotypes of *ap2m-2* (Yamaoka et al. 2013). Intriguingly, although the expression of AP2M-GFP in *ap2m-2* rescued the leaf and silique phenotypes (Supplemental Fig. S4, A and B) (Yamaoka et al. 2013), the roots of *pAP2M:AP2M-GFP/ap2m-2* plants were similar to those of the *aak1* mutant and were less wavy (Fig. 2, C to E; Supplemental Data Set 2), indicating that the C-terminally positioned GFP somehow modifies the function of AP2M in the root. In agreement with this notion, co-immunoprecipitation (Co-IP) analysis with *pAP2M:AP2M-GFP/ap2m-2* and *pAP2S:AP2S-GFP/ap2s* transgenic Arabidopsis revealed that the endogenous AAK1 copurified with AP2S-GFP, but not with AP2M-GFP (Supplemental Fig. S2C). Hence, the GFP tag disabled the interaction of AAK1 with AP2M-GFP, possibly the reason for the roots of *pAP2M:AP2M-GFP/ap2m-2* to behave like those of the *aak1* mutants.

AAK1 and AP2M regulate root touch responses

As root waving is a combined response to gravity and mechanical stimuli (Oliva and Dunand 2007), we investigated the touch response and medium penetration ability of *aak1* and *ap2m* roots by growing the seedlings horizontally on a medium containing different concentrations of agar (0.4%, 0.6%, 1%, and 1.2%). When grown horizontally on a medium supplemented with 0.4% agar, approximately half of the wild type roots penetrated the medium, whereas the root penetration of *aak1-1*, *aak1-2*, *aak1-3*, AAK1OE, and *ap2m-2* was reduced and that of *pAAK1:AAK1-GFP/aak1-1* plants slightly increased (Supplemental Fig. S5A). The root penetration of all genotypes was dramatically reduced when grown in 0.6% agar (Supplemental Fig. S5B), and almost none of the genotypes could penetrate 1% or 1.2% agar medium (Fig. 3, A and B; Supplemental Fig. S5C). When the roots were unable to penetrate 1% and 1.2% agar medium, three different root growth behaviors were observed: (i) a root growing continuously toward the gravity vector, causing detachment from the medium and the formation of an arch shape, defined as an "arch root"; mostly occurring in wild-type Col-0 (Fig. 3A; Supplemental Fig. S5D); (ii) a root growing wavily along the surface of the agar medium, typical of the *aak1* mutants, defined as a "wavy root" (Fig. 3A and Supplemental Fig. S5E); and (iii) a root growing along the surface of the agar with spiral curls, a distinct feature of the *ap2m-2* mutant, defined as a "curly root" (Fig. 3A;

Supplemental Fig. S5F). As roots had less chance to penetrate 1.2% agar than 1% agar, we performed the horizontal root growth assay on 1.2% agar medium, with reproducible results (Fig. 3, A and B).

When grown on 1.2% agar medium, approximately 88% of Col-0 roots were of the arch type, and approximately 10% were of the wavy root type (Fig. 3B). The roots of the *aak1-1*, *aak1-2*, and *aak1-3* mutants exhibited approximately 72% wavy, 24% arch, and 4% curly root types. The roots of *ap2m-2* and *aak1-1 ap2m-2* both displayed approximately 77% curly, 12% wavy, and 11% arch root types. Introduction of *pAAK1:AAK1-GFP* into *aak1-1* rescued the root behavior back to the wild-type, whereas the roots of AAK1OE displayed a root behavior between those of Col-0 and *aak1*, with 64% arch and 34% wavy root types (Fig. 3B). The above data indicate that AAK1 and AP2M play roles in the behavior of roots growing on an impenetrable surface, probably by modulating the gravitropic and touch responses.

Arabidopsis AAK1 regulates root behavior by phosphorylating AP2M on Thr-163

To assess the physiological function of AP2M phosphorylation, we introduced the phospho-null version of AP2M ($AP2M^{T163A}$) into the *ap2m* mutant. As *pAP2M:AP2M-GFP/ap2m-2* exhibited an *aak1*-like root phenotype in both the vertical (Fig. 2, C to E; Supplemental Data Set 2) and horizontal assays (Fig. 4, A and B), we inserted a tag-free version of AP2M into the *ap2m-3* mutant. In the root horizontal assay, *ap2m-3* displayed the same curly root type behavior as *ap2m-2* (Fig. 4, A and B). Introduction of the wild-type genomic DNA of *AP2M*, including the promoter region (*pAP2M:AP2M*), into the *ap2m-3* mutant not only rescued the leaf and silique phenotypes (Supplemental Fig. S4, G and H), but also reversed the curly back to arch root type as in the wild-type (Fig. 4, A and B), indicating that the tag-free version of AP2M fully rescued the *ap2m* phenotype. By contrast, even though the introduced phospho-null version of AP2M (*pAP2M:*$AP2M^{T163A}$) rescued the leaf and silique phenotypes (Supplemental Fig. S4, G and H), the root behavior of *pAP2M:*$AP2M^{T163A}$*/ap2m-3* resembled that of the *aak1* mutants, whose roots bent and grew along the agar surface (Fig. 4, A and B). These results imply that the phosphorylation state of AP2M plays a critical role in controlling root behavior, which could be a combined result of the crosstalk between root gravitropic and touch responses.

We next tested whether the kinase activity of AAK1 is required for the root behavior on hard agar surfaces. We introduced the kinase-dead versions of AAK1 under the control of the endogenous promoter (*pAAK1:*$AAK1^{K57A}$ and *pAAK1:*$AAK1^{D157A}$) into *aak1-1* and analyzed the root phenotypes of three homozygous lines for each kinase-dead construct. As expected, none of the AAK1 kinase-dead versions rescued the root behavior of *aak1-1* (Supplemental Fig. S6, A and B), demonstrating that the kinase activity of AAK1 is essential for its physiological function *in planta*.

To demonstrate the importance of Thr-163 phosphorylation in AP2M, we introduced two phospho-mimic forms of AP2M (*pAP2M:*$AP2MT^{163D}$ and *pAP2M:*$AP2MT^{163E}$) and a phospho-null form of AP2M (*pAP2M:*$AP2M^{T163A}$) into the *aak1-1* mutant. By screening 12 independent T2 heterozygous lines for each construct using the root horizontal assay, we found that 10 out of 12 lines of *pAP2M:*$AP2MT^{163E}$*/aak1-1* and 7 out of 12 lines of *pAP2M:*$AP2MT^{163D}$*/aak1-1* complemented *aak1* (Supplemental Fig. S7A). By contrast, the 12 *pAP2M:*$AP2MT^{163A}$*/aak1-1* lines still had a wavy root behavior (Supplemental Fig. S7A). We further analyzed two independent transgenic lines for each construct: *pAP2M:*$AP2M^{T163A}$*/aak1-1* (lines #1 and #2), *pAP2M:*$AP2M^{T163D}$*/aak1-1* (lines #1 and #2), and *pAP2M:*$AP2M^{T163E}$*/aak1-1* (lines #1 and #2) (Fig. 4, C and D). The roots of *pAP2M:*$AP2MT^{163D}$*/aak1-1* and *pAP2M:*$AP2MT^{163E}$*/aak1-1* behaved like the wild-type, but those of the *pAP2M:*$AP2MT^{163A}$*/aak1-1* lines still behaved like the *aak1* mutants (Fig. 4, C and D), indicating that the phospho-mimic forms of AP2M rescued the *aak1-1* phenotype, whereas the phospho-null form of AP2M did not. Quantitative reverse transcription PCR (RT-qPCR) analysis of *AP2M* transcripts in the transgenic lines (*AP2M*, $AP2M^{T163A}$, $AP2M^{T163D}$, and $AP2M^{T163D}$) in a different background (*ap2m-3* and *aak1-1*) confirmed that the root behavior was associated with the mutated AP2M versions, not with the *AP2M* expression levels (Supplemental Fig. S7B).

In summary, Arabidopsis AAK1 regulates root behavior in response to impenetrable surfaces via the phosphorylation of AP2M on Thr-163.

Phosphorylation of AP2M on Thr-163 by AAK1 regulates the endocytosis rate

Mutation of the phosphorylated threonine (T156A) in the human μ2 subunit has been shown to inhibit transferrin uptake in tissue cultures (Olusanya et al. 2001). Therefore, we examined whether endocytosis is affected in the *aak1* mutants and transgenic Arabidopsis expressing the phospho-null mutant AP2M protein in the *ap2m-3* background by monitoring FM4-64 uptake. Unexpectedly, whereas the *ap2m-2* and *ap2m-3* mutants exhibited obviously reduced FM4-64 uptake in root epidermal cells, FM4-64 uptake was not reduced in *aak1-1*, *aak1-2*, and *pAP2M:*$AP2M^{T163A}$*/ap2m-3* (Fig. 5, A and B; Supplemental Data Set 2), but rather was slightly higher than that of the wild-type. The FM4-64 uptake did not significantly differ between the wild-type and AAK1OE, and the introduction of *pAP2M:AP2M* into *ap2m-3* rescued the FM4-64 uptake to the wild-type level (Fig. 5, A and B; Supplemental Data Set 2). These results indicate that the unphosphorylated AP2M is still functional in Arabidopsis and that AAK1 is likely required to tune down endocytosis.

In addition, we noticed that, although most of the FM4-64 internalization events were similar between the wild-type and *aak1* mutants, a small population of cells showed elevated FM4-64 uptake (Fig. 5B; Supplemental Data Set 2).

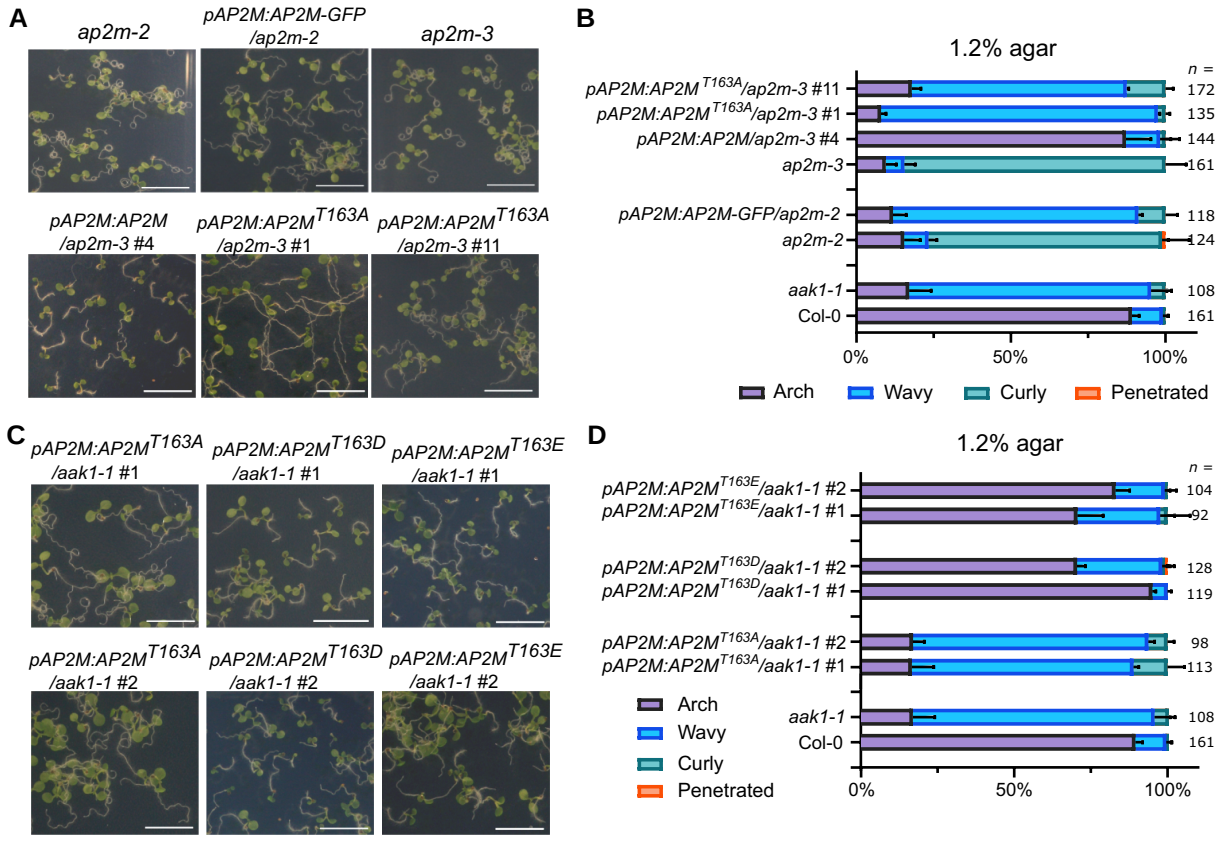

Figure 4. AP2M phosphorylation on Thr-163 by AAK1 regulates root behavior. **A)** Representative images of the root horizontal assay examining the root behavior of 7-day-old seedlings of *ap2m-2*, *ap2m- 3*, and the complemented lines with different AP2M versions, *pAP2M:AP2M-GFP/ap2m-2*, *pAP2M:AP2M/ap2m-3* (line #4), and *pAP2M:AP2M^{T163A}/ap2m-3* (lines #1 and #11). T3 generation seedlings homozygous for the transgenes were analyzed. **B)** Quantification of the root behavior of each genotype as in **A)**. Col-0 and *aak1-1* were used as controls. Three independent experiments were combined. **C)** Representative images of the root horizontal assay on 7-day-old seedlings of *aak1-1* expressing the phospho-mimic AP2M (*pAP2M:AP2M^{T163D}/aak1-1* and *pAP2M:AP2M^{T163E}/aak1-1*) and the phospho-null AP2M (*pAP2M:AP2M^{T163A}/aak1-1*). Two independent T2 lines for each construct were analyzed. Seedlings (homozygous or heterozygous for the transgenes) were chosen based on fluorescent seed selection. **D)** Quantification of the root behavior of each genotype as in **C)**. Three independent experiments were combined. Col-0 and *aak1-1* were used as controls and were the same as in **B)** because the experiments were done together. Error bars in **B** and **D)** represent the standard error (SE) of the three replicates. *n*, number of roots. Scale bar, 1 cm **A** and **C)**.

Therefore, we carried out a more detailed analysis of the population distributions. First, via a normality test, we found that the FM4-64 uptake rates of most genotypes, except *ap2m-2*, were not normally distributed (Supplemental Fig. S8), suggesting that judging the FM4-64 uptake rates by means of the average (arithmetic mean) values might not be fully representative. Therefore, we plotted the relative frequency distribution histograms and found that the FM4-64 uptake distributions of *aak1-1*, *aak1-2*, and *pAP2M:AP2M^{T163A}/ap2m-3* were flatter and wider than those of the others (Fig. 5C). Nonlinear curve fitting showed that the FM4-64 uptake distribution of the wild-type had two peaks, a major and a minor one centered at 0.36 and 0.58, respectively. The results of the *pAP2M:AP2M/ap2m-3* complementation line were similar, namely, with a major and minor peak at 0.39 and 0.61, respectively (Fig. 5C), but the fitted curves of *ap2m-2* and *ap2m-3* were more symmetric and had single peaks at 0.29 and 0.28, respectively (Fig. 5C). Interestingly, the distributions of *aak1-1*, *aak1-2*, and *pAP2M:AP2M^{T163A}/ap2m-3* were multimodal, with three peaks: *aak1-1* had two major peaks centered at 0.37 and 0.52 and one minor peak centered at 0.71; *aak1-2* had two major peaks at 0.37 and 0.54 and one minor peak at 0.76; and *pAP2M:AP2M^{T163A}/ap2m-3* had two major peaks at 0.38 and 0.53 and one minor peak at 0.71 (Fig. 5C). The extra minor peaks with higher ratios of FM4-64 internalization were the reason for the significantly higher average values than those of the wild-type, only when the sample size was large enough. By contrast, the distribution of AAK1OE was log-normal, with one geometric mean at 0.38, indicating that, albeit no significant differences were detected in the averages by the Kruskal–Wallis test (Fig. 5B; Supplemental Data Set 2), endocytosis was weakly affected in AAK1OE cells.

To examine whether CME of different PM cargos is affected by the absence of AAK1, we investigated the

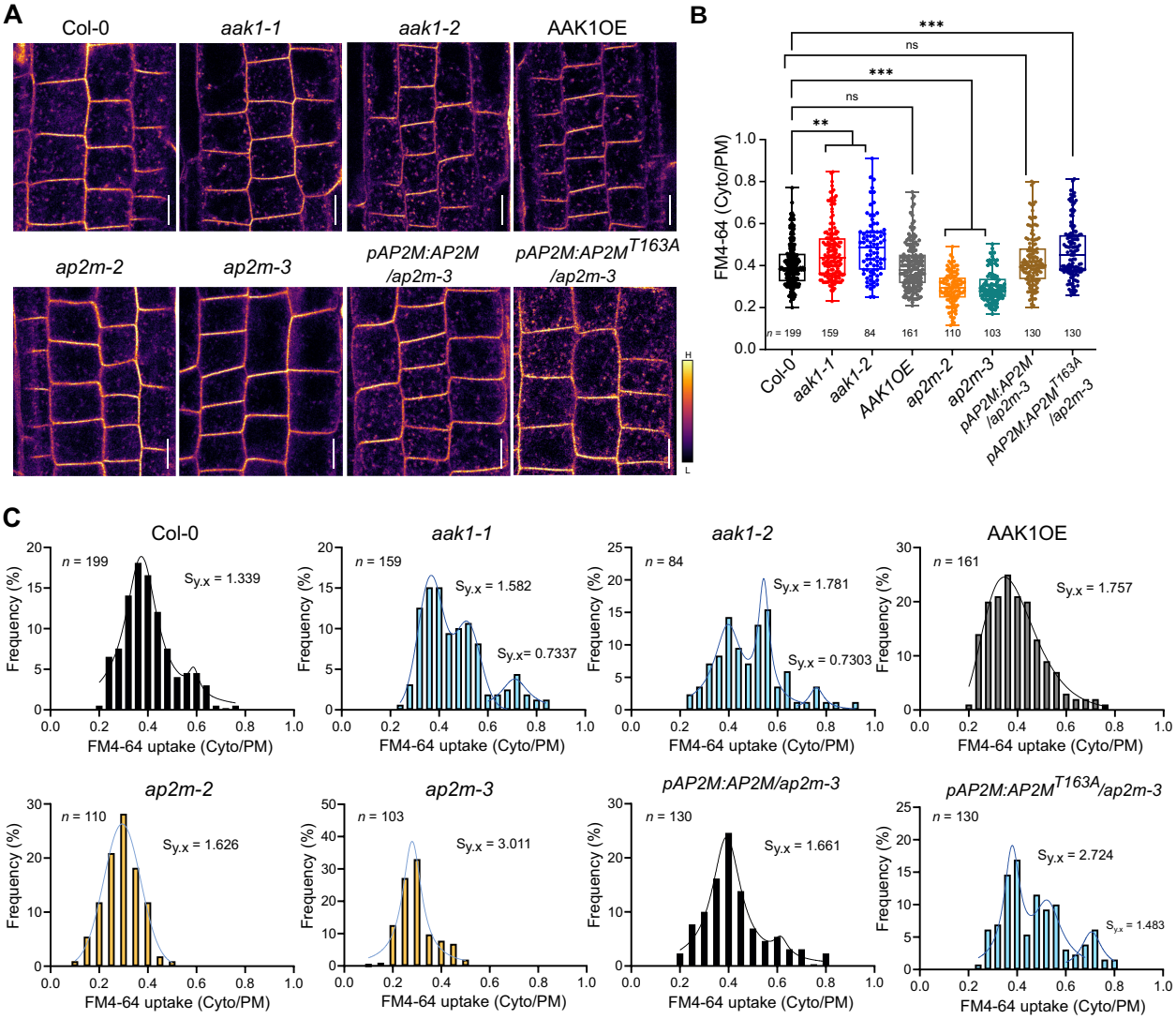

Figure 5. Phosphorylation of AP2M by AAK1 affects FM4-64 endocytosis. **A)** FM4-64 uptake in wild-type (Col-0), *aak1-1*, *aak1-2*, the AAK1 overexpression line (*p35S:AAK1-GFP*/Col-0, AAK1OE), *ap2m-2*, *ap2m-3*, *pAP2M:AP2M/ap2m-3* (line #4), and *pAP2M:AP2M^{T163A}/ap2m-* 3 (line #1). Five-day-old root epidermal cells were imaged after staining with FM4-64 (2 μM) for 10 min. Scale bars, 10 μm. **B)** Relative cytoplasmic (Cyto) to PM fluorescence intensity ratio of FM4-64 of the images in **A)**. The borders of the boxes represent the 25th to 75th percentiles, the center horizontal line indicates the median, and the whiskers indicate the minimum and the maximum values. All individual values are plotted. $^{**}P \leq 0.01$, $^{***}P \leq 0.001$ (Kruskal–Wallis nonparametric one-way ANOVA); ns, not significant. **C)** Frequency distribution graphs showing the ranges of FM4-64 uptake in the root epidermal cells of the different genotypes in **B)**. The bin widths for best-fit were set at 0.04 for Col-0, *aak1-1*, *aak1-2*, AAK1OE, and *pAP2M:AP2M^{T163A}/ap2m-3* (line #1) and at 0.05 for *ap2m-2*, *ap2m-3*, and *pAP2M:AP2M/ap2m-3* (line #4) by GraphPad Prism. The curves were fitted by nonlinear regression with either Gaussian, Lorentzian, or Log-normal functions, according to the least standard deviation of the residuals (Sy.x) values for goodness-of-fit. *n*, number of cells analyzed **B** and **C)**.

internalization of the fluorescent brassinosteroid (BR) analog Alexa Fluor 647-castasterone (AFCS), which is a ligand of the BR-INSENSITIVE1 (BRI1) receptor (Irani et al. 2012; Di Rubbo et al. 2013), in root cells of the *aak1-1* mutant. Comparable to the patterns of FM4-64 uptake, the rate of AFCS internalization was slightly higher in *aak1-1* than that of Col-0 (Fig. 6, A and B; Supplemental Data Set 2). The frequency distribution of AFCS endocytosis in Col-0 was more centered than that in *aak1-1*, which had a higher deviation (Fig. 6C). Similarly, the cytoplasmic versus PM fluorescence intensity ratio of another CME cargo, PIN2-GFP (the auxin efflux carrier PIN-FORMED2 fused to GFP) (Kitakura et al. 2011; Adamowski et al. 2018) was slightly higher in root cells of *aak1-1* versus the wild-type (Fig. 6, D to F; Supplemental Data Set 2). In addition, the accumulation of PIN2-GFP in Brefeldin A (BFA)-induced compartments (so-called BFA bodies) in *aak1-1* increased compared to the wild-type (Fig. 6, G and H; Supplemental Data Set 2). However, no significant differences in BFA body dissipation after the BFA washout were observed between the wild-type and *aak1-1*

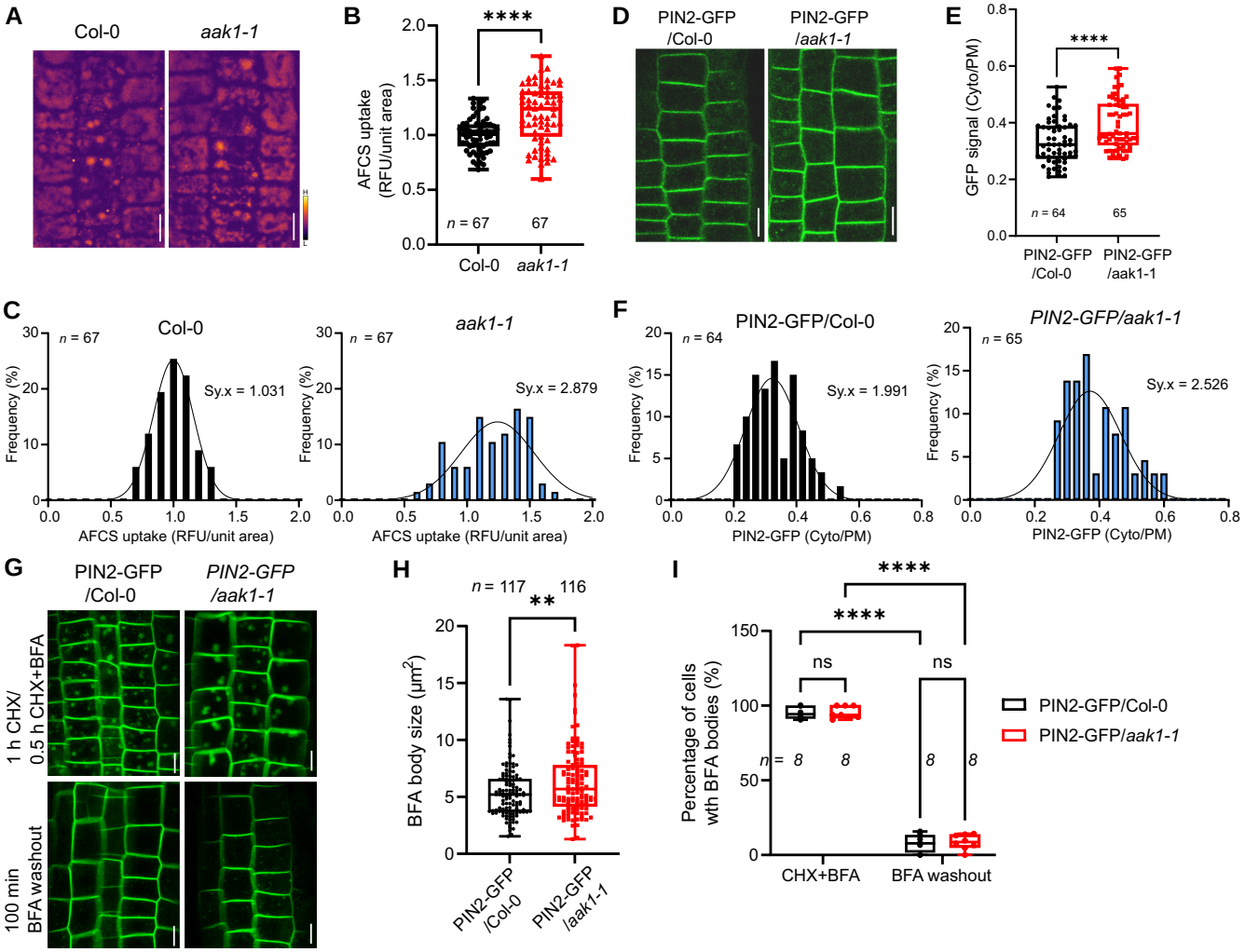

Figure 6. AAK1 regulates the endocytosis of BRI1 and PIN2. **A)** AFCS uptake in the root epidermal cells of 4-day-old Col-0 and *aak1-1*. Roots were pulsed with AFCS (30 μM) for 40 min, washed, and chased for 20 min before imaging. **B)** Quantification of AFCS fluorescence intensity in the vacuoles of the root cells of Col-0 and *aak1-1*. RFU, relative fluorescence units. ****$P \leq 0.0001$ (Welch's *t*-test). *n*, number of unit area. **C)** Frequency distributions showing the ranges of AFCS uptake in the root epidermal cells of Col-0 and *aak1-1*. The bin widths were set to 0.1. The curves were fitted by nonlinear regression with the Gaussian function for the least standard deviation of the residuals (Sy.x) value. *n*, number of unit area. **D)** Confocal images of *pPIN2:PIN-GFP* in the root epidermal cells of 5-day-old Col-0 and *aak1-1* seedlings. **E)** Relative cytoplasmic (Cyto) versus PM fluorescence intensity of PIN2-GFP of the images in **D)**. *n*, number of cells. **F)** Frequency distributions showing the ranges of the Cyto/PM ratio of PIN2-GFP in the root epidermal cells of Col-0 and *aak1-1*. The bin widths were set to 0.03. **G)** Accumulation of PIN2-GFP in the root cells of 5-day-old wild-type and *aak1-1* after Brefeldin A (BFA) treatment and after BFA washout. Seedlings were pretreated with cycloheximide (CHX) (50 μM, 1 h) followed by a co-treatment with CHX (50 μM) and BFA (50 μM) for 30 min. Seedlings were washed with medium containing CHX (50 μM) and imaged 100 min after the wash. **H)** BFA body sizes before the washout are shown in **G)**. *n*, number of BFA bodies. I, Percentage of BFA body-containing cells in PIN2-GFP seedlings before and after BFA washout shown in **G)**. The borders of boxes in **B**, **E**, **H**, and **I)** represent the 25th to 75th percentiles, the center horizontal line indicates the median, and the whiskers indicate the minimum and the maximum values. All individual values are plotted. *n*, number of roots. **$P \leq 0.01$, ****$P \leq 0.0001$ (Welch's *t*-test (**E** and **H**) and two-way ANOVA (**I**)), ns, not significant. Scale bars, 10 μm (**A**, **D**, and **G**).

mutant (Fig. 6, G and I; Supplemental Data Set 2), implying that AAK1 regulates PIN2 endocytosis, but not recycling, possibly to control its polar localization in the Arabidopsis root meristem (Supplemental Fig. S4, D and E; Supplemental Data Set 2).

Taken together, we conclude that Arabidopsis AAK1 controls the CME homeostasis of different PM cargoes in the root and thus affects its gravitropic and touch responses.

Discussion

In mammalian cells, the AP-2 complex is essential for CCV formation, and the null *ap2m* mutant in mouse is embryonic lethal (Collins et al. 2002; Mitsunari et al. 2005). In Arabidopsis, although AP-2 is required for efficient CME, the *ap2m* and *ap2s* mutants are viable, albeit with defects in leaf morphology, staminal filament elongation, pollen tube growth, and silique

development (Fan et al. 2013; Kim et al. 2013; Yamaoka et al. 2013). Nonetheless, the roles of AP-2 in root growth and development have been unclear. Here, we report that the primary root of the *ap2m* null mutant grew faster than the wild-type but displayed agravitropic, wavy, and skewing phenotypes during the seedling stage. When grown on impenetrable horizontal plates, the primary root of the *ap2m* mutant had a curly root behavior, distinct from that of the wild-type. These root phenotypes are probably due to defective endocytosis in root cells, which disturbs polar auxin transport (Dhonukshe et al. 2007; Men et al. 2008; Kitakura et al. 2011).

Our previous AP interactome studies discovered an association between AP-2 and an unknown kinase that is similar to the mammalian AAK1 (Wang et al. 2023). The roles of mammalian AAK1 in phosphorylating the μ2 subunit of AP-2 on a threonine residue (Thr-156) and in regulating AP-2 activity have been widely reported but also debated (Olusanya et al. 2001; Conner and Schmid 2002; Ricotta et al. 2002; Höning et al. 2005; Partlow et al. 2019; Wrobel et al. 2019). Although several lines of evidence suggest that Thr-156 phosphorylation in μ2 is required for cargo recognition via a phosphorylation-activated conformational change that promotes cargo and membrane binding (Olusanya et al. 2001; Collins et al. 2002; Ricotta et al. 2002; Höning et al. 2005), this hypothesis somehow conflicts with the temporal ordering of CCV formation, because AP-2 should have bound to the PM and the cargo before its phosphorylation by AAK1 (Wrobel et al. 2019). Moreover, AP-2 has been shown to bind to PtdIns(4,5)P2- and cargo-containing membranes without being phosphorylated, and the Thr-156 phosphorylation of μ2 not to have a major effect on the cargo affinity of AP-2 (Jackson et al. 2010; Kelly et al. 2014; Kadlecova et al. 2016; Wrobel et al. 2019). Instead, μ2 phosphorylation increases its affinity to ADAPTIN EAR-BINDING COAT-ASSOCIATED PROTEINS (NECAPs) and is the key determinant of the timing and recruitment of NECAP-1 in the AP-2 regulatory cycle, thus, modulating CCV formation and CME (Partlow et al. 2019; Wrobel et al. 2019).

Analysis of the AP interactome in Arabidopsis also identified a putative NECAP-1 homolog that interacts with AP-1 and AP-2 subunits (Wang et al. 2023). In mammalian systems, the recently identified active open+ conformation of AP-2 and the co-regulation with NECAPs might explain some of the discrepancies (Kelly et al. 2014; Wrobel et al. 2019), although whether NECAPs play a positive or inhibitory role in AP-2 activation remains a matter of debate (Beacham et al. 2018; Partlow et al. 2019; Wrobel et al. 2019). Additionally, AAK1 could function redundantly with the NAK family kinases, such as the cyclin G-associated kinase (GAK) (Umeda et al. 2000) and the bone morphogenic protein (BMP)-inducible kinase (BIKE) (Sorrell et al. 2016), or it might have other functions (Conner and Schmid 2003; Henderson and Conner 2007). Interestingly, mammalian AAK1 is activated by clathrin (Conner et al. 2003) but clathrin binds to the already opened AP-2 form in the PM (Kelly et al. 2014). Currently, the mechanism of AAK1 activation is unclear. The substrate binding site of AAK1 has been suggested to possibly be blocked by its C-terminal region, which can be removed through clathrin binding (Jackson et al. 2003), but later evidence showed that clathrin can also activate the C-terminally truncated AAK1 (Conner et al. 2003). It has also been speculated that phosphorylation may regulate the AAK1 activity because there are several phosphorylation sites in the kinase domain of human AAK1 (Sorrell et al. 2016) and one site in that of Arabidopsis (Supplemental Fig. S1C) (Mergner et al. 2020). However, the activity of human AAK1 is not dependent on phosphorylation (Sorrell et al. 2016).

In human cells, AAK1 seemingly inhibits AP-2-dependent transferrin internalization both in vitro and in vivo (Conner and Schmid 2002, 2003), and μ2 phosphorylation might function in an inactivation process (Partlow et al. 2019). Silencing of *AAK1* did not induce changes in AP2M phosphorylation, transferrin uptake, or AP-2 distribution (Conner and Schmid 2003; Henderson and Conner 2007). Using amphiphilic styryl dyes such as FM4-64 that particularly imbed in the outer membranes with a specific phospholipid composition in both mammalian and plant cells (Richards et al. 2000; Van Gisbergen et al. 2008; Dason et al. 2010), distinct vesicle pools of endocytic routes can be labeled. In neurons, FM4-64 is sequestered into synaptic vesicles (Newton and Murthy 2006; Chen et al. 2008), whereas in plant cells, FM4-64 is taken up by CME, flotillin-mediated endocytosis, and bulk-flow endocytosis (Bolte et al. 2004; Baral et al. 2015). Our data show that the uptake of FM4-64 is enhanced in *aak1* mutants and that the frequency distribution is flatter than that of the wild-type. A similar trend was observed for two other plant CME cargoes, AFCS and PIN2-GFP. AFCS is a fluorescent BR analog that is internalized together with the BRI1 receptor (Irani et al. 2012), whereas PIN2 is an auxin efflux carrier that mediates auxin gradient formation in the Arabidopsis root via its polar PM localization in the cortex and epidermal cells and thus, directs root gravitropism. The establishment and maintenance of PIN2 polarity are controlled by CME (Kitakura et al. 2011; Adamowski et al. 2018). Conversely, although the average value of FM4-64 uptake in plants overproducing AAK1 was the same as that of the wild-type, the FM4-64 uptake distribution in these plants was slightly skewed to the left. Hence, Arabidopsis AAK1 might regulate endocytic homeostasis and play an inhibitory role in endocytosis, which is consistent with findings in mammals (Conner and Schmid 2002, 2003; Partlow et al. 2019).

Our phylogenetic analysis revealed that Arabidopsis *AAK1* is a single-copy gene and that no other kinase homolog is present in the Arabidopsis genome. The Arabidopsis *AAK1* knockout mutant displayed less root waving and a reduced gravitropic response on vertical plates, but an increased obstacle avoidance response on horizontal plates. In addition, the introduction of the kinase-dead versions of AAK1 in *aak1-1* failed to rescue the *aak1* phenotype, which was successfully rescued by the phospho-mimic but not the

phospho-null form of AP2M, suggesting that AAK1 may be the only kinase that phosphorylates AP2M at Thr-163 in Arabidopsis. Furthermore, expression of the phospho-null form of AP2M in the *ap2m-3* mutant resulted in an *aak1*-like behavior. The *aak1* and *ap2m* mutants also exhibited opposite root phenotypes when grown on vertical plates. Altogether, these data suggest that AAK1 negatively regulates AP-2 activity by phosphorylating AP2M on Thr-163. Next, by performing an in vitro kinase assay using isotope labeling, we demonstrated that Arabidopsis AAK1 can phosphorylate the Thr-163 residue in AP2M. However, this phosphorylation event was not identified by our MS analysis even though it had been previously detected *in planta*.

Plant root behavior is complex because it is the sum of the output of root tropic responses (e.g. gravitropism, thigmotropism, hydrotropism, and halotropism) and autonomous movement (such as circumnutation) (Eapen et al. 2005; Durham Brooks et al. 2010; Galvan-Ampudia et al. 2013; Jacobsen et al. 2021; Loshchilov et al. 2021). PIN-mediated polar auxin transport and ethylene signaling have been shown to regulate root gravitropism and mechanical responses (Růžička et al. 2007; Yamamoto et al. 2008; Zhang and Friml 2020; Jacobsen et al. 2021), whereas abscisic acid and BRs play major roles in root hydrotropism (Eapen et al. 2005; Dietrich et al. 2017; Miao et al. 2018). The root behaviors of the *aak1* and *ap2m* mutants in the vertical and horizontal assays are probably due to the altered gravitropism and touch responses, because root gravitropic bending is affected in the mutants, and the main factors in the assays are the agar concentration and the plate orientation. A similar root horizontal assay and root behaviors have been reported but were not used to identify mutants (Tojo et al. 2021). Nonetheless, we cannot exclude the possibility that hydrotropism and drought avoidance also contribute to root behaviors, because the water potential of the medium decreases linearly with increasing agar concentration (Ghashghaie et al. 1991).

As endocytosis is essential for many cellular functions and signaling cascades, changes in the balance between endocytosis and another vesicle trafficking may disturb the dynamics of receptors and transporters on the PM, in turn affecting phytohormone signaling pathways (Dhonukshe et al. 2007; Kitakura et al. 2011; Di Rubbo et al. 2013; Xia et al. 2019; Liu et al. 2020), with modified root tropic responses and behaviors as a consequence. In the wild-type, when the Thr-163 of AP2M is phosphorylated by AAK1, endocytosis is regulated, and the roots exhibit normal gravitropic responses when grown vertically on the agar surface and pointed toward the gravitropic vector even when encountering the impenetrable medium. In the absence of AP2M, the endocytosis rates in the root cells are reduced, resulting in agravitropic and curly roots on vertical and horizontal plates, respectively. When only unphosphorylated AP2M is present in the cells, e.g. in the *aak1* null mutants, *AP2M-GFP/ap2m-2*, and *AP2M*^{T163A}*/ap2m-3*, the balance and coordination of endocytosis in the root cells are affected, leading to reduced root gravitropic bending and an enhanced obstacle avoidance response on vertical and horizontal plates, respectively.

In summary, we revealed the regulatory mechanisms of the AP-2 accessory protein AAK1 on AP2M phosphorylation in Arabidopsis, i.e. AAK1 phosphorylates AP2M on Thr-163, and this phosphorylation maintains the balance of endocytosis in root cells and controls root behaviors. Our findings suggest that AAK1 fine-tunes the functions of AP2M in root cells. How the phosphorylation of AP2M regulates endocytosis in plant cells and modulates root tropisms remains to be determined.

Materials and methods

Plant materials and growth conditions

Arabidopsis thaliana accession Columbia-0 plants were used for all experiments. The seeds were surface sterilized by chlorine gas and sown on half-strength Murashige and Skoog (½MS) solid plates (2.15 g/L MS salt (Duchefa), 10 g/L sucrose (Chem-Lab), 0.1 g/L myo-inositol (Sigma-Aldrich), 0.5 g/L MES (Duchefa), pH 5.7) with different concentrations of agar as indicated. The plates were vernalized at 4 °C in the dark for 3 days. Seeds were germinated and grown at 22 °C and a 16 h light/8 h dark photoperiod, under a standard light intensity (110 μmol m^{-2} s^{-1}) using full-spectrum fluorescent light bulbs, for 5, 7, or 10 days, either vertically or horizontally, according to the experiments. For all vertical experiments, the plates contained 1% (w/v) agar and were tilted at ∼15° from the vertical axis according to the plate rack design in the growth room. For horizontal experiments, the plates contained 1.2% (w/v) agar (except in Supplemental Fig. S5, 0.4%, 0.6%, and 1%) and were placed horizontally. The *aak1-1* (SALK_00168) mutant was obtained from the Arabidopsis Biological Resource Center. The transgenic Arabidopsis lines *pPIN2:PIN2-GFP*/Col-0 (Adamowski et al. 2018), *pAP2M:AP2M-GFP/ap2m-2* (Yamaoka et al. 2013), *pAP2S:AP2S-GFP/ap2s* (Fan et al. 2013), *p35S:GFP/Col-0* (Zhang et al. 2022), *ap2m-2* (Yamaoka et al. 2013), and *aux1-7* (Pickett et al. 1990) have been described previously.

Generation of constructs and transformation

For *pAAK1:AAK-GFP*, the 1873 bp promoter region and the genomic DNA of *AAK1* were first cloned into the Gateway entry vectors *pDNORp4p1r* and *pDONR221*, respectively, via Gateway BP reactions, and then subcloned with *pDONR P2r-P3-GFP* into the binary vector *pK7m34GW* (Karimi et al. 2005) by a Gateway LR reaction. For AAK1OE, the *gAAK1-pDONR221* entry clone was subcloned into *pK7FWG2* (Karimi et al. 2002) by an LR reaction to generate the *p35S:gAAK1-GFP* construct. For *pAAK1:nlsGFP*, *pAAK1-pDNORp4p1r* was subcloned into the expression vector *pMK7S*NFm14GW* (Karimi et al. 2007). For *pAAK1:AAK1*^{K57A} and *pAAK1:AAK1*^{D157A}, the *pAAK1-pDNORp4p1r*

and *gAAK1-pDONR221* entry clones were first subcloned into the *pH7m24GW* (Karimi et al. 2007) binary vector and then mutated by site-directed mutagenesis with the primers listed in Supplemental Table S1. For *pAP2M:AP2M*, the genomic DNA of *AP2M*, including its 2083bp promoter region, was cloned into *pGGC000* and then further mutated by site-directed mutagenesis to generate *pAP2M:AP2M^{T163A}-pGGC000*, *pAP2M:AP2M^{T163D}-pGGC000*, and *pAP2M:AP2M^{T163E}-pGGC000*. The entry clones were subcloned into the binary vector *pFASTRK-AG* with *pGG-A-LinkerIII-C* and *pGG-D-NOST-G* (Houbaert et al. 2018; Decaestecker et al. 2019) by the Golden Gate system (Karimi and Jacobs 2021). The constructs were first transferred to *Agrobacterium tumefaciens* C58C1 strain pMP90 and then transformed into Arabidopsis Col-0, *aak1-1*, or *ap2m-3* by the floral dip method.

For the CRISPR/Cas9 constructs, four and two gRNAs that target the first and last exons of *AAK1* and the first exon of *AP2M*, respectively, were designed using "CCtop" software (https://cctop.cos.uni-heidelberg.de:8043/). The four *AAK1* gRNAs (Supplemental Table S1) were cloned into the entry vectors *pGG-C-AtU6-26-BbsI-ccdB-BbsI-D*, *pGG-D-AtU6-26-BbsI-ccdB-BbsI-E*, *pGG-E-AtU6-26-BbsI-ccdB-BbsI-F*, and *pGG-F-AtU6-26-BbsI-ccdB-BbsI-G*, and the two *AP2M* gRNAs (Supplemental Table S1) into *pGG-E-AtU6-26-BbsI-ccdB-BbsI-F* and *pGG-F-AtU6-26-BbsI-ccdB-BbsI-G*, according to the previously described protocol (Decaestecker et al. 2019). The CRISPR/Cas9 expression constructs were generated by assembling the *AAK1* gRNA and the *AP2M* gRNA entry clones with *pGG-A-linkerIII-E-C* and *pGG-A-linkerIII-E-G*, respectively, into the backbone vector *pFASTRK-Atcas9-AG* (Blomme et al. 2022) by the Golden Gate reaction. The expression constructs were transferred to *Agrobacterium tumefaciens* C58C1 and then transformed into Arabidopsis Col-0 by the floral dip method. For genotyping, the genomic DNA sequence of *AAK1* and *AP2M* of the transgenic plants were amplified by PCR with the primers listed in Supplemental Table S1.

For protein purification, the constructs for GST-AP2M, GST-AP2A1, and GST-AP2S have been described previously (Liu et al. 2020). The MBP-AAK1 and GST-AP2M-T163 constructs and the GST-AP2M-T163A construct were cloned into *pOPINM* and *pOPINJ*, respectively, by in-fusion cloning (Berrow et al. 2007) with the primers listed in Supplemental Table S1.

Root phenotype assays

For the root waving assay (Fig. 1C), seedlings were grown vertically on ½MS plates with 1% (w/v) agar with a 15° tilted angle for 5 days. A wave was defined as a root turning angle of less than 120°. The waving numbers of individual roots were divided by their root length to obtain the waving number/cm ratio (Lanza et al. 2012).

Root horizontal assay

For the root horizontal assay, seedlings were grown on horizontal plates with 1.2% (w/v) agar for 7 days. The root penetration assay (Supplemental Fig. S5) was carried out in plates containing 0.4%, 0.6%, and 1% (w/v) agar, and the plants were grown horizontally. An arch root was defined as a root with more than half of it detached from the surface, whereas a wavy root was defined as a root with more than half of it growing wavily along the surface and a curly root as a root containing at least one 360° turn.

Gravistimulation of plants

Five-day-old seedlings grown vertically in the light on ½MS medium were gravistimulated by a 90° rotation in the vertical plane. The angle of the root tips deviating from the old gravity vector was measured at 0, 3, 6, 9, and 24 h after gravistimulation with ImageJ software (http://rsb.info.nih.gov/ij/).

Protein purification

The MBP-AAK1, GST-AP2M, GST-AP2A1, GST-AP2S, GST-AP2M-T163, and GST-AP2M-T163A constructs were transformed into competent *Escherichia coli* BL21 (DE3) cells, and the transformed cells were cultured in Luria–Bertani medium supplemented with 100 mg/mL carbenicillin at 37 °C to an optical density of 0.6. Expression was induced by the addition of 0.2 mM isopropyl β-D-1-thiogalactopyranoside (IPTG) at 16 °C overnight or 1 mM IPTG at 37 °C for 3 h (for GST-AP2M-T163 and GST-AP2M-T163A). The cells were harvested by centrifugation at 6,000 × *g*. For MBP-AAK1, the cells were resuspended in lysis buffer (20 mM Tris–HCl, 200 mM NaCl, 1 mM EDTA, 1 mM dithiothreitol, 200 μM phenylmethylsulfonyl fluoride, and protease inhibitors (Roche), pH 7.4) and lysed by sonication. MBP-AAK1 and GST-tagged proteins were purified with amylose resin (New England Biolabs) and with glutathione Sepharose 4B GST-tagged protein purification resin (GE Healthcare), respectively, according to the standard manufacturers' protocols.

Liquid chromatography with tandem mass spectrometry analysis for phospho-peptide detection

Peptides were redissolved in 20 μL loading solvent A (0.1% (v/v) trifluoroacetic acid in water/acetonitrile (98:2 (v/v)), of which 5 μL was injected for liquid chromatography with tandem mass spectrometry (LC-MS/MS) analysis on an Ultimate 3000 RSLC nano LC (Thermo Fisher Scientific) connected in-line to a Q Exactive mass spectrometer (Thermo Fisher Scientific). The peptides were first loaded on an in-house made trapping column (100 μm internal diameter (I.D.) × 20 mm, 5 μm beads C18 Reprosil-HD (Dr. Maisch, Ammerbuch-Entringen, Germany)). After the peptides had been flushed from the trapping column, they were separated on a 50 cm micro-pillar array collumn (μPAC) with C18-endcapped functionality (Pharmafluidics, Ghent, Belgium) kept at a constant temperature of 35 °C. Peptides were eluted by a linear gradient from 98% (v/v) solvent A′ (0.1% (v/v) formic acid in water) to 55% (v/v) solvent B′ (0.1% (v/v) formic acid in water/acetonitrile, 20/80 (v/v)) in

30 min at a flow rate of 300 nL/min, followed by a 5 min wash reaching 99% (v/v) solvent B′.

The mass spectrometer was operated in data-dependent, positive ionization mode, automatically switching between MS and MS/MS acquisition for the five most abundant peaks in a given MS spectrum. The source voltage was 3.2 kV and the capillary temperature was 275 °C. One MS1 scan (m/z 400 to 2,000, automatic gain control (AGC) target 3×10^6 ions, maximum ion injection time 80 ms), acquired at a resolution of 70,000 (at 200 m/z), was followed by up to five tandem MS scans (resolution 17,500 at 200 m/z) of the most intense ions fulfilling predefined selection criteria (AGC target 5×10^4 ions, maximum ion injection time 80 ms, isolation window 2 Da, fixed first mass 140 m/z, centroid as spectrum data type, intensity threshold 1.3×10^4, one exclusion of unassigned, >8 positively charged precursors, peptide match preferred, "exclude isotopes" on, dynamic exclusion time 12 s). The higher-energy collision dissociation was set to 25% of the normalized collision energy, and the polydimethylcyclosiloxane background ion at 445.120025 Da was used for internal calibration (lock mass). The raw files were processed with MaxQuant software (version 1.6.10.43) (Cox and Mann 2008), and searched with the built-in Andromeda search engine against the Araport11plus database that contains contaminating sequences, e.g. tags, keratins, and trypsin. Search parameters can be found in Supplemental Data Set 1.

In vitro kinase assay

Recombinant proteins were incubated in kinase reaction buffer (50 mM Tris–HCl, pH 7.5, 100 mM NaCl, 10 mM $MgCl_2$, and 10 μM ATP) in the presence of 5 µCi (γ-^{32}P)-ATP (NEG502A001MC; Perkin-Elmer) at 25 °C for 60 min. The reactions were terminated by adding NuPAGE LDS sample buffer (Invitrogen) and NuPAGE sample-reducing agent (Invitrogen), separated by 4% to 20% sodium dodecyl sulfate-polyacrylamide gel electrophoresis (SDS-PAGE), and stained with Coomassie Brilliant Blue. The gels were dried and radioactivity was detected by autoradiography on a photographic film with an FLA 5100 phosphor imager (Fujifilm).

Co-immunoprecipitation assay

For Co-IP in Arabidopsis, seeds were germinated and grown on ½MS. Ten-day-old seedlings were harvested and ground into a powder with liquid nitrogen. The fine powder was resuspended in extraction buffer (50 mM Tris–HCl, pH 7.5, 150 mM NaCl, 0.5% (v/v) NP-40, and a complete EDTA-free protease inhibitor cocktail (Roche)). The extracts were centrifuged at 18,000 × g at 4 °C for 10 min. The supernatants were transferred to new 2-ml tubes and centrifuged for an additional 10 min. After centrifugation, the supernatants were incubated with GFP-trap magnetic agarose (Chromotek) at 4 °C for 1 h. The beads were washed 3 times with 1 mL wash buffer (20 mM Tris–HCl, pH 7.5, 150 mM NaCl, 0.25% (v/v) NP-40) and then eluted with 80 μL elution buffer containing 1× NuPAGE LDS Sample Buffer (Thermo Fisher Scientific) and 1× NuPAGE Reducing Agent (Thermo Fisher Scientific) and heated at 60 °C for 10 min.

SDS-PAGE and immunoblotting

Total protein extracts were obtained by grinding the plant materials into a fine powder in liquid nitrogen. The powder was resuspended in extraction buffer (50 mM Tris–HCl, pH 7.5, 150 mM NaCl, 0.5% (v/v) NP-40, and a cOmplete EDTA-free protease inhibitor cocktail (Roche)). The extracts were centrifuged at 18,000 × g at 4 °C for 10 min. The supernatants were transferred to new 2-ml tubes and centrifuged for an additional 10 min. The protein extracts were boiled in sample buffer (1× NuPAGE LDS sample buffer, 1× NuPAGE reducing agent (Thermo Fisher Scientific)) for 10 min at 60°C and loaded on a 4% to 20% (w/v) Mini-PROTEAN TGX Precast Protein Gel (Bio-Rad). The proteins were separated by electrophoresis and blotted onto a membrane with trans-Blot Turbo Mini 0.2 μm Nitrocellulose Transfer Packs (Bio-Rad). The membranes were blocked overnight at 4 °C in 5% (w/v) skimmed milk dissolved in 25 mM Tris–HCl (pH 8), 150 mM NaCl, and 0.05% (v/v) Tween20. The blots were then incubated at room temperature with the monoclonal α-GFP antibody (1:5,000) (Miltenyi Biotec, 130-091-833), α-tubulin antibody (1:5,000) (Sigma-Aldrich, T5168), and α-AAK1 antibody (1:5,000). The α-AAK1 antibody was a custom antibody generated by Eurogentec (Seraing, Belgium) using the antigen: QRYGNSKMRENQKTA.

Quantitative RT-PCR

RNA was extracted from 7-day-old seedlings with the ReliaPrep RNA Miniprep System (Promega). Of the purified RNA, 1 μg was amplified in a reverse transcriptase reaction with a qScript XLT 1-Step RT-PCR Kit (Quantabio). Subsequently, qPCR was performed with SYBR Green master mix (Roche) using gene-specific primers designed to amplify *AP2M*. *ACTIN2* was used as the normalization reference. Primers are listed in Supplemental Table S1.

Chemical treatments

For subcellular localization of AAK1-GFP, 4-day-old *pAAK1:AAK1-GFP/aak1-1* seedlings were treated with 50 μM BFA (50 mM stock in dimethyl sulfoxide; Sigma-Aldrich) and 2 μM (*N*-(3-triethylammoniumpropyl)-4-(6-(4-(diethylamino) phenyl) hexatrienyl) pyridinium dibromide) (FM4-64; 2 mM stock in purified water; Invitrogen) in ½MS liquid medium without sucrose for 30 min before confocal imaging. For FM4-64 uptake experiments, 4-day-old seedlings were incubated in ½MS liquid medium without sucrose containing 2 M FM4-64 for 10 min before confocal imaging. For PIN2-GFP recycling experiments, 5-day-old seedlings were pretreated with cycloheximide (CHX) (50 μM, 1 h) followed by a co-treatment with CHX (50 μM) and BFA (50 μM) in ½MS liquid medium for 30 min. Seedlings were subsequently washed with medium containing CHX (50 μM) for 100 min.

Confocal microscopy and image analysis

All confocal images were acquired with a Leica SP8X confocal microscope with the gating system (0.3 to 6 ns) application for autofluorescence removal. GFP, FM4-64, and AFCS were excited by a white laser. The excitation and detection window settings were: GFP, 488/500 to 530 nm; FM4-64, 515/570 to 670 nm; and AFCS, 635/655 to 755 nm. For FM4-64 uptake and PIN2-GFP internalization and recycling experiments, images were captured on the cell cortex layer of the epidermal cells at the root transition zone with a laser configuration without saturated signals. The fluorescent PM intensity and intracellular space were measured with ImageJ to quantify FM4-64 uptake and the PIN2-GFP signal. The PM and intracellular spaces of individual cells were selected with a brush tool size of 5 pixels and the polygon selection tool, and histograms of pixel intensities were generated. The average intensity of the top 100 highest pixels based on the histogram for both the PM and the intracellular space was used to calculate the cytoplasm/PM ratios (Ortiz-Morea et al. 2016; Liu et al. 2020). BFA body size and BFA body number were measured as described previously (Luo et al. 2015). The polarity of PIN2-GFP signals was calculated by determining the mean values of defined PM-areas at the apical and lateral sides of the root epidermis or the basal and lateral sides of the root cortex cells as described previously (Kakar et al. 2013). For the AFCS experiments, the fluorescence intensities from the region of interest (ROI) of a maximum projected stack of eight slices, 1.5 μm apart, were quantified and normalized to the area as previously described (Irani et al. 2014). For kymographs of AAK1-GFP and AP2S-GFP, endocytic foci in vivo were measured with an Ultra View Vox Spinning disc confocal imaging system (Perkin-Elmer), running on the Volocity software package mounted on an Eclipse Ti inverted microscope (Nikon) with a Plan Apo Lambda 100× oil; numerical aperture, 1.45 corrected lens and third-generation perfect focus system (PFSIII) for Z-drift compensation. Time series were acquired at two time points per second intervals for 2 min. Excitation was done with a solid-state 488 nm diode-pumped solid-state laser (50 mW) (Perkin-Elmer). Kymographs were generated with a line thickness of 3.

Phylogenetic analysis

To construct the phylogenetic tree, amino acid sequences were obtained from the NCBI database based on ortholog calling using the BLASTp program. Sequences were aligned using Clustal Omega (Sievers et al. 2011) with default parameters. A maximum-likelihood phylogenetic tree was constructed using PhyML 3.0 (Guindon et al. 2010) with 100 bootstrap replicates. Alignment and tree files used for phylogenetic analysis are provided as Supplemental Files 1 and 2.

Statistical analysis

All statistical analyses and graph generations were done with GraphPad Prism .8 software. Kruskal–Wallis one-way analysis of variance (ANOVA) with Dunnett's multiple comparisons was applied for the statistical tests. The relative frequency distribution histograms were created by means of the frequency distribution function in column analyses with a bin width of 0.04 for *aak1-1*, *aak1-2*, AAK1OE, and *pAP2M:AP2M*^{T163A}*/ap2m-3* and 0.05 for *ap2m-2*, *ap2m-3*, and *pAP2M:AP2M/ap2m-3*, automatically chosen by GraphPad Prism based on best-fit. The curve fitting was analyzed by nonlinear regression in XY analyses with a distribution function fitting better with the frequency distribution according to the least $S_{y.x}$ value for goodness-of-fit. Statistical data are provided in Supplemental Data Set 2.

Accession numbers

Sequence data from this article can be found in the GenBank/EMBL/TAIR data libraries under the following accession numbers. Arabidopsis genes: *AAK1* (AT2G32850), *AP2M* (AT5G46630), *AP2S* (AT1G47830), *NECAP-1* (AT3G58600), *PIN2* (AT5G57090). For phylogenetic analysis and amino acid alignment of human genes: *AAK1* (Q2M2I8), *BIKE* (Q9NSY1), *GAK* (O14976), *AP2M1* (Q96CW1). For yeast genes: *ALK1* (P43633), *ENV7* (Q12003). For mouse genes: *AAK1* (Q3UHJ0), *BIKE* (Q91Z96), *GAK* (Q99KY4), *MPSK* (O88697). For fruit fly genes: *PSK* (Q9VI84), *NAK* (Q9VJ30), *Auxilin* (Q9VMY8). For nematode genes: *gakh-1* (Q20483), *sel-5* (G5ECQ3). For Chlamydomonas gene: CR07G02400 (A0A2K3DJ59). For Brassica genes BR03G16570 (M4E2C4), BR05G11370 (M4CMW4). For maize genes: ZM02G25990 (A0A1D6Q3X3), ZM05G32400 (A0A1D6HBX6); ZM04G17600 (K7U1D6), ZM08G11310 (A0A3L6DLW1). For rice genes: OS09G10720 (XP_015612326.1), OS02G37880 (XP_015627128). For soybean (*Glycine max*) genes: GM08G15921 (K7L6T7), GM15G42460 (I1MJK2). For the tomato (*Solanum lycopersicum*) gene: SL01G074010 (XP_004229357).

Acknowledgments

We thank I. Hara-Nishimura (Konan University, Japan) and J. Lin (Beijing Forestry University, China) for providing published materials, L. Sterck and S. M. Kao (VIB-UGent, Belgium) for help with phylogenetic analysis, X. Xu, D. Eeckhout and G. De Jaeger (VIB-UGent, Belgium) for help with MS analyses and useful discussions, D. Van Damme and P. Grones (VIB-UGent, Belgium) for critical reading of the manuscript, and M. De Cock for help in preparing it. This work was supported by the Research Foundation-Flanders projects (G008416N, G0E5718N, and 3G038020 to E.R.). X. Z. and P. W. are indebted to the China Scholarship Council for predoctoral fellowships. L. D. V. received a postdoctoral fellowship from the Special Research Fund (Bijzonder Onderzoeksfonds, Ghent University).

Author contributions

W.S., X.Z., and E.R. conceived the project. W.S. did most of the work. P.W. generated the *ap2m-3* mutant and performed the

kinetics of root gravitropism, qPCR analysis, and BFA washout experiment. X.Z. isolated the *aak1-1* mutant and generated the AAK1OE and *pAAK1:nlsGFP* lines. L.D.V. and I.D.S. analyzed and interpreted the MS data. W.S. and E.R. wrote the manuscript. All authors revised the manuscript.

Supplemental data

The following materials are available in the online version of this article.

Supplemental Figure S1. Sequence conservation and domain organization of AAK1.

Supplemental Figure S2. AP2M is phosphorylated and AAK1 copurified with AP2S-GFP, but not with AP2M-GFP.

Supplemental Figure S3. Expression and localization of AAK1 in Arabidopsis.

Supplemental Figure S4. Phenotypes of *aak1* and *ap2m* mutants.

Supplemental Figure S5. Root penetration assay and root behavior.

Supplemental Figure S6. The kinase-dead AAK1 did not rescue the root phenotype of *aak1-1*.

Supplemental Figure S7. The phospho-mimic forms of AP2M rescue the root behavior of *aak1-1*.

Supplemental Figure S8. FM4-64 uptake.

Supplemental Table S1. Primer list.

Movie 1. Subcellular localization of AAK1-GFP in root and cotyledon cells.

Supplemental Data Set 1. Phospho-peptide analysis of the AP2M-T163A peptide.

Supplemental Data Set 2. Statistical data analysis.

Supplemental File 1. Alignment used for phylogenetic analysis.

Supplemental File 2. Tree file for phylogenetic analysis.

Conflict of interest statement. None declared.

Data availability

All data needed to evaluate the conclusions in this article are available in the article and in its online supplementary material. Additional data related to this article will be shared on reasonable request to the corresponding author.

References

Adamowski M, Narasimhan M, Kania U, Glanc M, De Jaeger G, Friml J. A functional study of AUXILIN-LIKE1 and 2, two putative clathrin uncoating factors in Arabidopsis. Plant Cell. 2018:**30**(3):700–716. https://doi.org/10.1105/tpc.17.00785

Agajanian MJ, Walker MP, Axtman AD, Ruela-de-Sousa RR, Serafin DS, Rabinowitz AD, Graham DM, Ryan MB, Tamir T, Nakamichi Y, et al. WNT Activates the AAK1 kinase to promote clathrin-mediated endocytosis of LRP6 and establish a negative feedback loop. Cell Rep. 2019:**26**(1):79–93.e8. https://doi.org/10.1016/j.celrep.2018.12.023

Baral A, Irani NG, Fujimoto M, Nakano A, Mayor S, Mathew MK. Salt-induced remodeling of spatially restricted clathrin-independent endocytic pathways in Arabidopsis root. Plant Cell. 2015:**27**(4):1297–1315. https://doi.org/10.1105/tpc.15.00154

Beacham GM, Partlow EA, Lange JJ, Hollopeter G. NECAPs are negative regulators of the AP2 clathrin adaptor complex. eLife. 2018:**7**(1):e32242. https://doi.org/10.7554/eLife.32242

Berrow NS, Alderton D, Sainsbury S, Nettleship J, Assenberg R, Rahman N, Stuart DI, Owens RJ. A versatile ligation-independent cloning method suitable for high-throughput expression screening applications. Nucleic Acids Res. 2007:**35**(6):e45. https://doi.org/10.1093/nar/gkm047

Blomme J, Develtere W, Köse A, Arraiza Ribera J, Brugmans C, Jaraba-Wallace J, Decaestecker W, Rombaut D, Baekelandt A, Fernández Fernández ÁD, et al. The heat is on: a simple method to increase genome editing efficiency in plants. BMC Plant Biol. 2022:**22**(1):142. https://doi.org/10.1186/s12870-022-03519-7

Bolte S, Talbot C, Boutte Y, Catrice O, Read ND, Satiat-Jeunemaitre B. FM-dyes as experimental probes for dissecting vesicle trafficking in living plant cells. J Microsc. 2004:**214**(2):159–173. https://doi.org/10.1111/j.0022-2720.2004.01348.x

Borner GHH, Antrobus R, Hirst J, Bhumbra GS, Kozik P, Jackson LP, Sahlender DA, Robinson MS. Multivariate proteomic profiling identifies novel accessory proteins of coated vesicles. J Cell Biol. 2012:**197**(1):141–160. https://doi.org/10.1083/jcb.201111049

Chen X, Barg S, Almers W. Release of the styryl dyes from single synaptic vesicles in hippocampal neurons. J Neurosci. 2008:**28**(8):1894–1903. https://doi.org/10.1523/JNEUROSCI.4518-07.2008

Collins BM, McCoy AJ, Kent HM, Evans PR, Owen DJ. Molecular architecture and functional model of the endocytic AP2 complex. Cell. 2002:**109**(4):523–535. https://doi.org/10.1016/S0092-8674(02)00735-3

Conner SD, Schmid SL. Identification of an adaptor-associated kinase, AAK1, as a regulator of clathrin-mediated endocytosis. J Cell Biol. 2002:**156**(5):921–929. https://doi.org/10.1083/jcb.200108123

Conner SD, Schmid SL. Differential requirements for AP-2 in clathrin-mediated endocytosis. J Cell Biol. 2003:**162**(5):773–779. https://doi.org/10.1083/jcb.200304069

Conner SD, Schröter T, Schmid SL. AAK1-mediated μ2 phosphorylation is stimulated by assembled clathrin. Traffic. 2003:**4**(12):885–890. https://doi.org/10.1046/j.1398-9219.2003.0142.x

Cox J, Mann M. MaxQuant enables high peptide identification rates, individualized p.p.b.-range mass accuracies and proteome-wide protein quantification. Nat Biotechnol. 2008:**26**(12):1367–1372. https://doi.org/10.1038/nbt.1511

Dason JS, Smith AJ, Marin L, Charlton MP. Vesicular sterols are essential for synaptic vesicle cycling. J Neurosci. 2010:**30**(47):15856–15865. https://doi.org/10.1523/JNEUROSCI.4132-10.2010

Decaestecker W, Buono RA, Pfeiffer ML, Vangheluwe N, Jourquin J, Karimi M, Van Isterdael G, Beeckman T, Nowack MK, Jacobs TB. CRISPR-TSKO: a technique for efficient mutagenesis in specific cell types, tissues, or organs in Arabidopsis. Plant Cell. 2019:**31**(12):2868–2887. https://doi.org/10.1105/tpc.19.00454

Dhonukshe P, Aniento F, Hwang I, Robinson DG, Mravec J, Stierhof Y-D, Friml J. Clathrin-mediated constitutive endocytosis of PIN auxin efflux carriers in *Arabidopsis*. Curr Biol. 2007:**17**(6):520–527. https://doi.org/10.1016/j.cub.2007.01.052

Di Rubbo S, Irani NG, Kim SY, Xu Z-Y, Gadeyne A, Dejonghe W, Vanhoutte I, Persiau G, Eeckhout D, Simon S, et al. The clathrin adaptor complex AP-2 mediates endocytosis of BRASSINOSTEROID INSENSITIVE1 in *Arabidopsis*. Plant Cell. 2013:**25**(8):2986–2997. https://doi.org/10.1105/tpc.113.114058

Dietrich D, Pang L, Kobayashi A, Fozard JA, Boudolf V, Bhosale R, Antoni R, Nguyen T, Hiratsuka S, Fujii N, et al. Root hydrotropism is controlled via a cortex-specific growth mechanism. Nat Plants. 2017:**3**(6):17057. https://doi.org/10.1038/nplants.2017.57

Durham Brooks TL, Miller ND, Spalding EP. Plasticity of Arabidopsis root gravitropism throughout a multidimensional condition space quantified by automated image analysis. Plant Physiol. 2010:**152**(1):206–216. https://doi.org/10.1104/pp.109.145292

Eapen D, Barroso ML, Ponce G, Campos ME, Cassab GI. Hydrotropism: root growth responses to water. Trends Plant Sci. 2005:**10**(1):44–50. https://doi.org/10.1016/j.tplants.2004.11.004

Fan L, Hao H, Xue Y, Zhang L, Song K, Ding Z, Botella MA, Wang H, Lin J. Dynamic analysis of *Arabidopsis* AP2 σ subunit reveals a key role in clathrin-mediated endocytosis and plant development. Development. 2013:**140**(18):3826–3837. https://doi.org/10.1242/dev.095711

Galvan-Ampudia CS, Julkowska MM, Darwish E, Gandullo J, Korver RA, Brunoud G, Haring MA, Munnik T, Vernoux T, Testerink C. Halotropism is a response of plant roots to avoid a saline environment. Curr Biol. 2013:**23**(20):2044–2050. https://doi.org/10.1016/j.cub.2013.08.042

Ghashghaie J, Brenckmann F, Saugier B. Effects of agar concentration on water status and growth of rose plants cultured in vitro. Physiol Plant. 1991:**82**(1):73–78. https://doi.org/10.1111/j.1399-3054.1991.tb02904.x

Guindon S, Dufayard JF, Lefort V, Anisimova M, Hordijk W, Gascuel O. New algorithms and methods to estimate maximum-likelihood phylogenies: assessing the performance of PhyML 3.0. Syst Biol. 2010:**59**(3):307–321. https://doi.org/10.1093/sysbio/syq010

Gupta-Rossi N, Ortica S, Meas-Yedid V, Heuss S, Moretti J, Olivo-Marin J-C, Israël A. The adaptor-associated kinase 1, AAK1, is a positive regulator of the Notch pathway. J Biol Chem. 2011:**286**(21):18720–18730. https://doi.org/10.1074/jbc.M110.190769

Henderson DM, Conner SD. A novel AAK1 splice variant functions at multiple steps of the endocytic pathway. Mol Biol Cell. 2007:**18**(7):2698–2706. https://doi.org/10.1091/mbc.e06-09-0831

Höning S, Ricotta D, Krauss M, Späte K, Spolaore B, Motley A, Robinson M, Robinson C, Haucke V, Owen DJ. Phosphatidylinositol-(4,5)-bisphosphate regulates sorting signal recognition by the clathrin-associated adaptor complex AP2. Mol Cell. 2005:**18**(5):519–531. https://doi.org/10.1016/j.molcel.2005.04.019

Houbaert A, Zhang C, Tiwari M, Wang K, de Marcos Serrano A, Savatin DV, Urs MJ, Zhiponova MK, Gudesblat GE, Vanhoutte I, et al. POLAR-guided signalling complex assembly and localization drive asymmetric cell division. Nature. 2018:**563**(7732):574–578. https://doi.org/10.1038/s41586-018-0714-x

Irani NG, Di Rubbo S, Mylle E, Van den Begin J, Schneider-Pizoń J, Hniliková J, Šíša M, Buyst D, Vilarrasa-Blasi J, Szatmári AM, et al. Fluorescent castasterone reveals BRI1 signaling from the plasma membrane. Nat Chem Biol. 2012:**8**(6):583–589. https://doi.org/10.1038/nchembio.958

Irani NG, Di Rubbo S, Russinova E. In vivo imaging of brassinosteroid endocytosis in Arabidopsis. In: **Otegui MS**, editor. Plant endosomes. New York: Springer; 2014. p. 107–117

Jackson AP, Flett A, Smythe C, Hufton L, Wettey FR, Smythe E. Clathrin promotes incorporation of cargo into coated pits by activation of the AP2 adaptor μ2 kinase. J Cell Biol. 2003:**163**(2):231–236. https://doi.org/10.1083/jcb.200304079

Jackson LP, Kelly BT, McCoy AJ, Gaffry T, James LC, Collins BM, Höning S, Evans PR, Owen DJ. A large-scale conformational change couples membrane recruitment to cargo binding in the AP2 clathrin adaptor complex. Cell. 2010:**141**(7):1220–1229. https://doi.org/10.1016/j.cell.2010.05.006

Jacobsen AGR, Jervis G, Xu J, Topping JF, Lindsey K. Root growth responses to mechanical impedance are regulated by a network of ROS, ethylene and auxin signalling in Arabidopsis. New Phytol. 2021:**231**(1):225–242. https://doi.org/10.1111/nph.17180

Kadlecova Z, Spielman SJ, Loerke D, Mohanakrishnan A, Reed DK, Schmid SL. Regulation of clathrin-mediated endocytosis by hierarchical allosteric activation of AP2. J Cell Biol. 2016:**216**(1):167–179. https://doi.org/10.1083/jcb.201608071

Kakar K, Zhang H, Scheres B, Dhonukshe P. CLASP-mediated cortical microtubule organization guides PIN polarization axis. Nature. 2013:**495**(7442):529–533. https://doi.org/10.1038/nature11980

Karimi M, Bleys A, Vanderhaeghen R, Hilson P. Building blocks for plant gene assembly. Plant Physiol. 2007:**145**(4):1183–1191. https://doi.org/10.1104/pp.107.110411

Karimi M, De Meyer B, Hilson P. Modular cloning in plant cells. Trends Plant Sci. 2005:**10**(3):103–105. https://doi.org/10.1016/j.tplants.2005.01.008

Karimi M, Inzé D, Depicker A. GATEWAY^{TM} Vectors for *Agrobacterium*-mediated plant transformation. Trends Plant Sci. 2002:**7**(5):193–195. https://doi.org/10.1016/S1360-1385(02)02251-3

Karimi M, Jacobs TB. GoldenGateway: a DNA assembly method for plant biotechnology. Trends Plant Sci. 2021:**26**(1):95–96. https://doi.org/10.1016/j.tplants.2020.10.004

Kelly BT, Graham SC, Liska N, Dannhauser PN, Höning S, Ungewickell EJ, Owen DJ. AP2 controls clathrin polymerization with a membrane-activated switch. Science. 2014:**345**(6195):459–463. https://doi.org/10.1126/science.1254836

Kim SY, Xu Z-Y, Song K, Kim DH, Kang H, Reichardt I, Sohn EJ, Friml J, Juergens G, Hwang I. Adaptor protein complex 2-mediated endocytosis is crucial for male reproductive organ development in *Arabidopsis*. Plant Cell. 2013:**25**(8):2970–2985. https://doi.org/10.1105/tpc.113.114264

Kirchhausen T, Owen D, Harrison SC. Molecular structure, function, and dynamics of clathrin-mediated membrane traffic. Cold Spring Harb Perspect Biol. 2014:**6**(5):a016725. https://doi.org/10.1101/cshperspect.a016725

Kitakura S, Vanneste S, Robert S, Löfke C, Teichmann T, Tanaka H, Friml J. Clathrin mediates endocytosis and polar distribution of PIN auxin transporters in *Arabidopsis*. Plant Cell. 2011:**23**(5):1920–1931. https://doi.org/10.1105/tpc.111.083030

Lanza M, Garcia-Ponce B, Castrillo G, Catarecha P, Sauer M, Rodriguez-Serrano M, Páez-García A, Sánchez-Bermejo E, Mohan TC, Leo del Puerto Y, et al. Role of actin cytoskeleton in brassinosteroid signaling and in its integration with the auxin response in plants. Dev Cell. 2012:**22**(6):1275–1285. https://doi.org/10.1016/j.devcel.2012.04.008

Liu D, Kumar R, Claus LAN, Johnson AJ, Siao W, Vanhoutte I, Wang P, Bender KW, Yperman K, Martins S, et al. Endocytosis of BRASSINOSTEROID INSENSITIVE1 is partly driven by a canonical Tyr-based motif. Plant Cell. 2020:**32**(11):3598–3612. https://doi.org/10.1105/tpc.20.00384

Loshchilov I, Del Dottore E, Mazzolai B, Floreano D. Conditions for the emergence of circumnutations in plant roots. PLoS One. 2021:**16**(5):e0252202. https://doi.org/10.1371/journal.pone.0252202

Luo Y, Scholl S, Doering A, Zhang Y, Irani NG, Di Rubbo S, Neumetzler L, Krishnamoorthy P, Van Houtte I, Mylle E, et al. V-ATPase activity in the TGN/EE is required for exocytosis and recycling in *Arabidopsis*. Nat Plants. 2015:**1**(7):15094. https://doi.org/10.1038/nplants.2015.94

McMahon HT, Boucrot E. Molecular mechanism and physiological functions of clathrin-mediated endocytosis. Nat Rev Mol Cell Biol. 2011:**12**(8):517–533. https://doi.org/10.1038/nrm3151

Men S, Boutté Y, Ikeda Y, Li X, Palme K, Stierhof Y-D, Hartmann M-A, Moritz T, Grebe M. Sterol-dependent endocytosis mediates post-cytokinetic acquisition of PIN2 auxin efflux carrier polarity. Nat Cell Biol. 2008:**10**(2):237–244. https://doi.org/10.1038/ncb1686

Mergner J, Frejno M, List M, Papacek M, Chen X, Chaudhary A, Samaras P, Richter S, Shikata H, Messerer M, et al. Mass-spectrometry-based draft of the *Arabidopsis* proteome. Nature. 2020:**579**(7799):409–414. https://doi.org/10.1038/s41586-020-2094-2

Mettlen M, Chen P-H, Srinivasan S, Danuser G, Schmid SL. Regulation of clathrin-mediated endocytosis. Annu Rev Biochem. 2018:**87**(1):871–896. https://doi.org/10.1146/annurev-biochem-062917-012644

Miao R, Wang M, Yuan W, Ren Y, Li Y, Zhang N, Zhang J, Kronzucker HJ, Xu W. Comparative analysis of Arabidopsis ecotypes reveals a role

for brassinosteroids in root hydrotropism. Plant Physiol. 2018:**176**(4): 2720–2736. https://doi.org/10.1104/pp.17.01563

Mitsunari T, Nakatsu F, Shioda N, Love PE, Grinberg A, Bonifacino JS, Ohno H. Clathrin adaptor AP-2 is essential for early embryonal development. Mol Cell Biol. 2005:**25**(21):9318–9323. https://doi.org/10.1128/MCB.25.21.9318-9323.2005

Newton J, Murthy V. Measuring exocytosis in neurons using FM labeling. J Vis Exp. 2006:**1**(1):117. https://doi.org/10.3791/117

Oliva M, Dunand C. Waving and skewing: how gravity and the surface of growth media affect root development in Arabidopsis. New Phytol. 2007:**176**(1):37–43. https://doi.org/10.1111/j.1469-8137.2007.02184.x

Olusanya O, Andrews PD, Swedlow JR, Smythe E. Phosphorylation of threonine 156 of the μ2 subunit of the AP2 complex is essential for endocytosis in vitro and in vivo. Curr Biol. 2001:**11**(11):896–900. https://doi.org/10.1016/S0960-9822(01)00240-8

Ortiz-Morea FA, Savatin DV, Dejonghe W, Kumar R, Luo Y, Adamowski M, Van den Begin J, Dressano K, Pereira de Oliveira G, Zhao X, et al. Danger-associated peptide signaling in *Arabidopsis* requires clathrin. Proc Natl Acad Sci U S A. 2016: **113**(39):11028–11033. https://doi.org/10.1073/pnas.1605588113

Partlow EA, Baker RW, Beacham GM, Chappie JS, Leschziner AE, Hollopeter G. A structural mechanism for phosphorylation-dependent inactivation of the AP2 complex. eLife. 2019:**8**(8): e50003. https://doi.org/10.7554/eLife.50003

Pelkmans L, Fava E, Grabner H, Hannus M, Habermann B, Krausz E, Zerial M. Genome-wide analysis of human kinases in clathrin- and caveolae/raft-mediated endocytosis. Nature. 2005:**436**(7047):78–86. https://doi.org/10.1038/nature03571

Pickett FB, Wilson AK, Estelle M. The *aux1* mutation of *Arabidopsis* confers both auxin and ethylene resistance. Plant Physiol. 1990:**94**(3):1462–1466. https://doi.org/10.1104/pp.94.3.1462

Richards DA, Guatimosim C, Betz WJ. Two endocytic recycling routes selectively fill two vesicle pools in frog motor nerve terminals. Neuron. 2000:**27**(3):551–559. https://doi.org/10.1016/S0896-6273(00)00065-9

Ricotta D, Conner SD, Schmid SL, von Figura K, Höning S. Phosphorylation of the AP2 μ subunit by AAK1 mediates high affinity binding to membrane protein sorting signals. J Cell Biol. 2002:**156**(5):791–795. https://doi.org/10.1083/jcb.200111068

Roth TF, Porter KR. Yolk protein uptake in the oocyte of the mosquito *Aedes aegypti* L. J Cell Biol. 1964:**20**(2):313–332. https://doi.org/10.1083/jcb.20.2.313

Růžička K, Ljung K, Vanneste S, Podhorská R, Beeckman T, Friml J, Benková E. Ethylene regulates root growth through effects on auxin biosynthesis and transport-dependent auxin distribution. Plant Cell. 2007:**19**(7):2197–2212. https://doi.org/10.1105/tpc.107.052126

Sievers F, Wilm A, Dineen D, Gibson TJ, Karplus K, Li W, Lopez R, McWilliam H, Remmert M, Söding J, et al. Fast, scalable generation of high-quality protein multiple sequence alignments using Clustal Omega. Mol Syst Biol. 2011:**7**(1):539. https://doi.org/10.1038/msb.2011.75

Sorrell FJ, Szklarz M, Abdul Azeez KR, Elkins JM, Knapp S. Family-wide structural analysis of human Numb-associated protein kinases. Structure. 2016:**24**(3):401–411. https://doi.org/10.1016/j.str.2015.12.015

Tojo H, Nakamura A, Ferjani A, Kazama Y, Abe T, Iida H. A method enabling comprehensive isolation of Arabidopsis mutants exhibiting unusual root mechanical behavior. Front Plant Sci. 2021:**12**(3): 646404. https://doi.org/10.3389/fpls.2021.646404

Traub LM. Tickets to ride: selecting cargo for clathrin-regulated internalization. Nat Rev Mol Cell Biol. 2009:**10**(9):583–596. https://doi.org/10.1038/nrm2751

Umeda A, Meyerholz A, Ungewickell E. Identification of the universal cofactor (auxilin 2) in clathrin coat dissociation. Eur J Cell Biol. 2000:**79**(5): 336–342. https://doi.org/10.1078/S0171-9335(04)70037-0

Van Gisbergen PAC, Esseling-Ozdoba A, Vos JW. Microinjecting FM4–64 validates it as a marker of the endocytic pathway in plants. J Microsc. 2008:**231**(2):284–290. https://doi.org/10.1111/j.1365-2818.2008.02041.x

Vu LD, Stes E, Van Bel M, Nelissen H, Maddelein D, Inzé D, Coppens F, Martens L, Gevaert K, De Smet I. Up-to-date workflow for plant (Phospho)proteomics identifies differential drought-responsive phosphorylation events in maize leaves. J Proteome Res. 2016:**15**(12): 4304–4317. https://doi.org/10.1021/acs.jproteome.6b00348

Wang P, Siao W, Zhao X, Arora D, Wang R, Eeckhout D, Kumar R, Houbaert A, De Winne N, et al. Adaptor protein complex interaction map in Arabidopsis identifies P34 as a common stability regulator. Nat Plants. 2023:**9**(2):355–371. https://doi.org/10.1038/s41477-022-01328-2

Willems P, Horne A, Van Parys T, Goormachtig S, De Smet I, Botzki A, Van Breusegem F, Gevaert K. The Plant PTM Viewer, a central resource for exploring plant protein modifications. Plant J. 2019:**99**(4):752–762. https://doi.org/10.1111/tpj.14345

Wrobel AG, Kadlecova Z, Kamenicky J, Yang JC, Herrmann T, Kelly BT, McCoy AJ, Evans PR, Martin S, Müller S, et al. Temporal ordering in endocytic clathrin-coated vesicle formation via AP2 phosphorylation. Dev Cell. 2019:**50**(4):494–508. https://doi.org/10.1016/j.devcel.2019.07.017

Xia L, Mar Marquès-Bueno M, Bruce CG, Karnik R. Unusual roles of secretory SNARE SYP132 in plasma membrane H^+-ATPase traffic and vegetative plant growth. Plant Physiol. 2019:**180**(2): 837–858. https://doi.org/10.1104/pp.19.00266

Yamamoto C, Sakata Y, Taji T, Baba T, Tanaka S. Unique ethylene-regulated touch responses of *Arabidopsis thaliana* roots to physical hardness. J Plant Res. 2008:**121**(5):509–519. https://doi.org/10.1007/s10265-008-0178-4

Yamaoka S, Shimono Y, Shirakawa M, Fukao Y, Kawase T, Hatsugai N, Tamura K, Shimada T, Hara-Nishimura I. Identification and dynamics of *Arabidopsis* adaptor protein-2 complex and its involvement in floral organ development. Plant Cell. 2013:**25**(8): 2958–2969. https://doi.org/10.1105/tpc.113.114082

Yoshinari A, Hosokawa T, Amano T, Beier MP, Kunieda T, Shimada T, Hara-Nishimura I, Naito S, Takano J. Polar localization of the borate exporter BOR1 requires AP2-dependent endocytosis. Plant Physiol. 2019:**179**(4):1569–1580. https://doi.org/10.1104/pp.18.01017

Zhang Y, Friml J. Auxin guides roots to avoid obstacles during gravitropic growth. New Phytol. 2020:**225**(3):1049–1052. https://doi.org/10.1111/nph.16203

Zhang C, Lauster T, Tang W, Houbaert A, Zhu S, Eeckhout D, De Smet I, De Jaeger G, Jacobs TB, Xu T, et al. ROPGAP-dependent interaction between brassinosteroid and ROP2-GTPase signaling controls pavement cell shape in *Arabidopsis*. Curr Biol. 2022:**32**(3): 518–531. https://doi.org/10.1016/j.cub.2021.12.043

Zulawski M, Braginets R, Schulze WX. PhosPhAt goes kinases—searchable protein kinase target information in the plant phosphorylation site database PhosPhAt. Nucleic Acids Res. 2013:**41**(D1): D1176–D1184. https://doi.org/10.1093/nar/gks1081